



universität  
wien

# MASTERARBEIT / MASTER'S THESIS

Titel der Masterarbeit / Title of the Master's Thesis

„Novel insights into the endocytic process of adipose stem cell derived extracellular vesicles in Schwann cells“

verfasst von / submitted by

Maximilian Härtinger, BSc

angestrebter akademischer Grad / in partial fulfilment of the requirements for the degree of

Master of Science (MSc)

Wien, 2021 / Vienna 2021

Studienkennzahl lt. Studienblatt /  
degree programme code as it appears on  
the student record sheet:

UA 066 877

Studienrichtung lt. Studienblatt /  
degree programme as it appears on  
the student record sheet:

Masterstudium Genetik und Entwicklungsbiologie

Betreut von / Supervisor:

Univ. Prof. Dr. Christine Radtke, MBA, FEBOPRAS

# Kurzfassung

In den letzten Jahren hat sich die Forschung auf dem Gebiet der Extrazelluläre Vesikel (EVs) erheblich weiterentwickelt, aber deren genaue Wirkungsweise in diversen biologischen Prozessen ist nachwievor nicht vollständig geklärt. Ein mögliches therapeutisches Anwendungsgebiet ist die Regeneration von Verletzungen der peripheren Nerven. Bei Neurotmesis muss chirurgisch interveniert werden, und je nach Defektgröße wird entweder spannungsfrei koaptiert oder fehlendes Gewebe ersetzt. Schwann-Zellen (SCs) wurden als Hauptakteure der peripheren Nervenregeneration identifiziert und sind daher ein vielversprechendes Ziel für neue therapeutische Ansätze. Mehrere Studien haben bereits über pro-regenerative Wirkungen von aus Fettstammzellen isolierten EVs (ASC-EVs) nach Internalisierung durch SCs berichtet.

Ziel dieser Studie ist es, die Internalisierung von ASC-EVs durch SCs zu charakterisieren. Zunächst wurde die Energieabhängigkeit der Internalisierung von EVs durch Kühlung sowie durch Hemmung der mitochondrialen Atmung festgestellt. Weiters wurden die SCs vor der Inkubation mit fluoreszenzmarkierten ASC-EVs mit Inhibitoren für Makropinozytose (MP) und Clathrinabhängiger Endozytose (CME) behandelt. Die Internalisierung wurde dann mit der bildgebenden Durchflusszytometrie analysiert, welche High-Throughput herkömmlicher Durchflusszytometrie mit den durch die Mikroskopie gewonnenen räumlichen Informationen kombiniert.

Die Inhibierung von CME verringerte die Internalisierung von ASC-EVs signifikant, blockierte den Membrantransit jedoch nicht vollständig. Dies indiziert, dass ASC-EVs in SCs hauptsächlich durch CME internalisiert werden, aber auch andere Zugangswege von ASC-EVs genutzt werden um in SCs zu gelangen. Um das volle Potenzial von EVs auszuschöpfen, ist es unerlässlich, die Interaktion mit den Zielzellen zu verstehen. Die Identifizierung des Hauptweges der Internalisierung ist ein weiterer Schritt auf dem Weg zu einer therapeutischen Anwendung von EVs.

**Keywords:** *Extrazelluläre Vesikel, Schwannzellen, Fettstammzellen, Periphere Nervenregeneration, Endozytose, Makropinozytose, Aufnahme*

# Abstract

In recent years, the field of extracellular vesicles (EVs) has significantly advanced, and possible EV involvement has been shown in a plethora of physiological and pathophysiological processes. Also, their possible regenerative applications have attracted special interest, especially in regeneration of severe peripheral nerve injuries. Proliferating Schwann cells (SCs) have been identified as the key players of peripheral nerve regeneration, and are therefore targeted in novel therapeutic approaches. Several studies have reported pro-regenerative effects of adipose stem cell derived extracellular vesicles (ASC-EVs) following internalization by SCs. To harness the full potential of EVs, it is imperative to understand the interaction with target cells. This study aims at characterizing the internalization of ASC-EVs by SCs. First, energy-dependency of EV internalization was established by applying a temperature block and inhibiting the mitochondrial respiration. Furthermore, SCs were treated with inhibitors for macropinocytosis (MP) and clathrin-mediated endocytosis (CME) prior to incubation with fluorescently labeled ASC-EVs. Internalization was then analyzed with imaging flow cytometry, combining high throughput analysis with spatial information gained by microscopy. The inhibition of CME significantly decreased the internalization of ASC-EVs, but did not completely block it, suggesting that SCs internalize ASC-EVs primarily, but not exclusively, by CME. Hence, additional modes of entry need to be explored. The modes of interaction and internalization of EVs are not sufficiently described yet. Nonetheless, the research field of EV biology is constantly growing, bringing together scientists from different genres, with the goal of understanding EVs and how to best employ them in regenerative medicine.

**Keywords:** *extracellular vesicles, Schwann cells, adipose stem cells, peripheral nerve regeneration, endocytosis, macropinocytosis, uptake*

# Acknowledgements

I would like to thank my supervisor Prof. Christine Radtke for her continuous support and for enabling me to conduct research in the field of peripheral nerve regeneration and extracellular vesicles. I would like to extend my sincere thanks to the team of Prof. Radtkes research laboratory at the Department of Plastic, Reconstructive and Aesthetic Surgery of the Medical University of Vienna for their insights, ideas suggestions and support. Additionally, I am grateful to Prof. Thomas Heuser and Sonja Jacob of the Electron Microscopy Facility at Vienna BioCenter Core Facilities (VBCF), member of the Vienna BioCenter (VBC), Austria, for their guidance and insights with Transmission Electron Microscopy and their fruitful cooperation. I also want to express my gratitude to Prof. Andreas Spittler and Günther Hofbauer (Center of Translational Research, Department of Surgery, Medical University of Vienna), who helped me with the Imaging Flow Cytometry. I am also grateful to Marion Gröger (Core Facility Imaging, Medical University of Vienna) for her technical support and insights regarding confocal microscopy.

# Contents

<b>Kurzfassung</b>	<b>i</b>
<b>Abstract</b>	<b>ii</b>
<b>Acknowledgements</b>	<b>iii</b>
<b>1 Introduction</b>	<b>1</b>
1.1 Peripheral nerve regeneration . . . . .	1
1.2 Extracellular vesicles . . . . .	2
1.2.1 Interaction with target cells . . . . .	3
1.2.2 EVs in regenerative medicine . . . . .	4
1.2.3 EVs in peripheral nerve regeneration . . . . .	5
1.3 Endocytosis . . . . .	5
1.3.1 Clathrin-mediated endocytosis . . . . .	5
1.3.2 Clathrin-independent endocytosis . . . . .	6
1.3.3 Macropinocytosis . . . . .	7
1.4 Rationale and importance of this study . . . . .	7
<b>2 Methods</b>	<b>8</b>
2.1 Animals . . . . .	8
2.2 Schwann cells . . . . .	8
2.2.1 Schwann cell isolation and culture . . . . .	8
2.2.2 Schwann cell characterization . . . . .	9
2.3 Adipose tissue derived stem cells . . . . .	9
2.3.1 Adipose tissue derived stem cell isolation and culture . . . . .	9
2.3.2 Adipose tissue derived stem cell characterization . . . . .	10
2.4 Adipose tissue derived stem cell extracellular vesicles . . . . .	11
2.4.1 Adipose tissue derived stem cell extracellular vesicle isolation . . . . .	11
2.4.2 Adipose tissue derived stem cell extracellular vesicle characterization . . . . .	11
2.5 ASC-EV internalization assay . . . . .	12
2.5.1 Fluorescent labeling of ASC-EVs . . . . .	12
2.5.2 Internalization verification and nuclear translocation . . . . .	12
2.5.3 Visualization of early-stage ASC-EV internalization . . . . .	13
2.5.4 Establishing energy-dependency of ASC-internalization . . . . .	13
2.5.5 Inhibitor cytotoxicity . . . . .	14

2.5.6	Endocytosis inhibitor treatment . . . . .	14
2.5.7	ASC-EV internalization assessment via imaging flow cytometry . . . . .	14
2.6	Statistical analysis . . . . .	15
<b>3</b>	<b>Results</b>	<b>15</b>
3.1	Characterization of SCs, ASCs and ASC-EVs . . . . .	15
3.1.1	Characterization of SCs . . . . .	15
3.1.2	Characterization of ASCs . . . . .	15
3.1.3	Characterization of ASC-EVs. . . . .	18
3.2	Internalization of ASC-EVs by SCs . . . . .	19
3.2.1	Internalization of ASC-EVs by SCs is energy-dependent . . . . .	22
3.2.2	Internalization of ASC-EVs by SCs is mostly mediated by clathrin . . . . .	22
<b>4</b>	<b>Discussion</b>	<b>24</b>
Outlook	. . . . .	27
	<b>Bibliography</b>	<b>29</b>
	<b>List of Figures</b>	<b>39</b>
	<b>Abbreviations</b>	<b>41</b>

# 1 Introduction

## 1.1 Peripheral nerve regeneration

Despite promising advances, regeneration of peripheral nerve injuries (PNI) still faces challenges and limitations. Where direct, tension-less coaptation is no longer possible due to the defect distance, the gold standard remains autologous grafting. This however comes with donor site morbidity and only moderate outcomes [1]. On the quest to find alternative therapeutic approaches, a deeper understanding of cellular processes underlying peripheral nerve regeneration is key.

Peripheral nerves have a complex hierarchical architecture, and consist of numerous axons clustered in specific subunits called fascicles [2]. The outermost sheath, termed epineurium, consists of dense connective tissue and ensheathes multiple nerve fascicles and accompanying vessels. Fascicles are bundles of axons surrounded by the perineurium, another layer of connective tissue. Peripheral nervous axons are ensheathed by a cuff of multiple layers of myelin containing plasma membrane, produced by the glial cells of the peripheral nervous system, Schwann cells (SCs). While larger diameter axons are myelinated individually, smaller diameter axons are ensheathed together.

PNI are categorized based on their severity and extent of damage to the nervous subunits [2,3]. Minor crush injuries often result in neuropraxia, with only partial damage to the myelin sheath, but intact the axon. More severely, in axonotmesis, the axon is severed, however, the surrounding connective tissue remains intact. PNIs where all nervous structures are disrupted including a complete transection of the axon, are termed neurotmesis. If the axon remains intact, spontaneous regeneration is expected [4]. If the axon is severed, a process called Wallerian degeneration is triggered [5], where the axon distal to the injury site is degraded, leading to the initiation of injury repair mechanisms. Here, SCs emerged as key players of the inert injury response and are in the focus of novel therapeutic approaches [6]. The plasticity of SCs enables them to change phenotype upon injury and create a microenvironment that promotes regeneration of the injured axon [5]. Transdifferentiated repair-phenotype SCs take up numerous roles, including myelin debris clearance and immunomodulation [7]. Nonetheless, it is the alignment of proliferating SCs into support structures termed bands of Bungner that put them into the spotlight. These aligned SCs provide structural and neurotrophic support for the regrowing axon, however, this support is short-lived as the lineage reprogramming is only transient, which limits the intrinsic regenerative capabilities [6,8,9].

Depending of the severity of the PNI, modern therapeutic approaches are trying to engage this problem by one of two ways: offering additional structural support, and/or cellular stimulation.

Structural support can be provided by auto-, allo- or xenografts of nerve tissue [10], or alternatively by conduits mimicking the endoneurial basal laminar tube. Here, a variety of biomaterials, such as spidersilk [11], are being employed as filling material, enhancing the mechanical guidance of regrowing structures. Additionally, conduits may be loaded with neurotrophic factors to enhance neuronal regeneration via cellular stimulation [10], or directly supplemented with SCs [12]. Highly proliferative cells such as adipose tissue derived stem cells (ASCs) have been shown to aid peripheral nerve regeneration, however, cell-based therapies underlie strict regulation and have biological limitations [13, 14]. Hence, an auspicious alternative to ASCs pose their signaling messengers, extracellular vesicles (EVs) [15]. ASC-EVs have been shown to increase SC proliferation *in vitro* [16], potentially prolonging the SC lineage reprogramming and thereby increasing the surmountable nerve gap distance. However, for a therapeutic application of EVs to come into fruition, there are still too many unknowns in EV biology [17], which will be discussed further below.

## 1.2 Extracellular vesicles

The advent of ultracentrifugation and electron microscopy in biology enabled the analysis of subcellular organelles and cell-derived phospholipid spherical vesicles. Initially described as “platelet dust” [18] and regarded as debris, the heterogenous population of signaling vehicles is now gathered under the umbrella term extracellular vesicles (EVs). Several classification systems have been suggested, however, nomenclature and classification based on the biogenesis of vesicles has prevailed. Hence, it is now commonly distinguished between microvesicles, exosomes and apoptotic bodies [19, 20]. Microvesicles are formed by outward budding of the plasma membrane and thus resemble the membrane composition of their parent cells closely. Ranging between 50 to 1000 nm in diameter, microvesicles carry bioactive cargo that includes coding and non-coding RNAs and cytoplasmic proteins [20]. Exosomes on the other hand originate from the endolysosomal pathway and are formed by inward budding of the multivesicular body (MVB) membrane [20,21]. Upon fusion of the MVB membrane with the cell membrane, exosomes are released into the extracellular space. Their biogenesis equips the exosomes with a unique set of identifiers that allow a distinction from microvesicles and other vesicles. The most commonly used identifiers are non-tissue specific transmembrane tetraspanins CD63 and CD81, as well as accessory proteins such as ALIX [22]. Compared to other vesicles, exosomes are rather small, with a diameter of 40-150 nm [19–21]. Additionally, apoptotic bodies originate from outward blebbing of the phospholipid membrane of cells undergoing apoptosis [23]. Their cargo however differs from microvesicles and exosomes, as it consists mainly of cellular fractions including nuclei fragments, organelles and chromatin remnants [23]. Apoptotic bodies may be distinguished due to their size of 500 nm upwards, as well as their extensive amounts of phosphatidylserine [20, 23]. Due to disputes about marker specificity, the International Society for Extracellular Vesicles (ISEV) proposed a nomenclature based on EVs’ properties, such as size ranges, cells of origin, or marker expression [22]. This study focuses on small EVs de-

rived from the endolysosomal pathway. EVs act as paracrine, pleiotropic signalosomes and are associated with development [24–29], homeostasis [30–33], regeneration [34, 35] and immune response [36–40] as well as pathological processes [32, 41–46]. An exhaustive description of EV involvements however remains to be fully characterized, as additional roles emerge constantly.

### 1.2.1 Interaction with target cells

The interaction of EVs with target cells still remains unsolved. Although numerous modes of interaction have been described, a common denominator could not be identified so far. According to the current understanding, interaction processes depend on both cells of origin as well as recipient cells [17, 19]. Figure 1 provides an overview of small EV biogenesis and possible modes of interaction with target cells. Additionally, the four hallmark characteristics of EVs are shown: 1) a lipid bilayer membrane, 2) cellular origin, 3) bioactive cargo, and 4) no means of replication. Exosomal signal transduction can be classified as either receptor-ligand interaction or molecular signal delivery [47]. Especially in the context of immunomodulation, EVs may interact superficially with target cells, for example in MHC cross-dressing [48] or T-cell activation [49]. Other signaling cascades that can be triggered by EVs include Notch, EGFRvIII and IFN- $\gamma$ /STAT [15]. In case of molecular signal delivery, multiple possibilities have been described. Bioactive EV cargo can be delivered to the target cell by fusion of the vesicular plasma membrane with the target cell membrane, thus releasing the cargo into the cytosol.

Similar to viral entry mechanisms, this process requires transmembrane synctin proteins as well as respective receptor molecules, and low pH conditions are favourable [15]. The cellular membrane is rearranged to accommodate hemifusion, followed by pore formation and cargo release. Of note, the vesicular membrane gets incorporated into the cellular membrane [50]. While membrane fusion is well-described, the current body of evidence suggests that it is not the main mode of EV interaction with target cells [47]. Instead, the majority of EV signaling likely involves internalization and subsequent translocation of EVs by target cells. Depleting EVs of their membrane proteins hinders EV uptake, indicating that internalization is dependent on specific protein-protein interactions. Of special interest are tetraspanins, a family of proteins that include CD9, CD63 and CD81, which are well-established EV markers. Due to their role in other processes such as cellular adhesion and vesicular fusion, tetraspanins are likely candidates for EV internalization mediators. Additional essential protein candidates are integrins, immunoglobulins, proteoglycans and lectins [51].

Furthermore, the internalization of EVs has been shown to be energy-dependent, as it is significantly inhibited at 4°C [51, 52]. By disrupting the actin cytoskeleton, EV internalization may also be inhibited, suggesting that cytoskeletal integrity is essential as well. Taken together, the most common mode of interaction with target cells seems to be internalization via endocytosis [51]. Endocytic internalization of EVs can be broken down into clathrin-dependent endocytosis (CDE), clathrin-independent endocytosis (CIE), and macropinocytosis (MP). The mode of

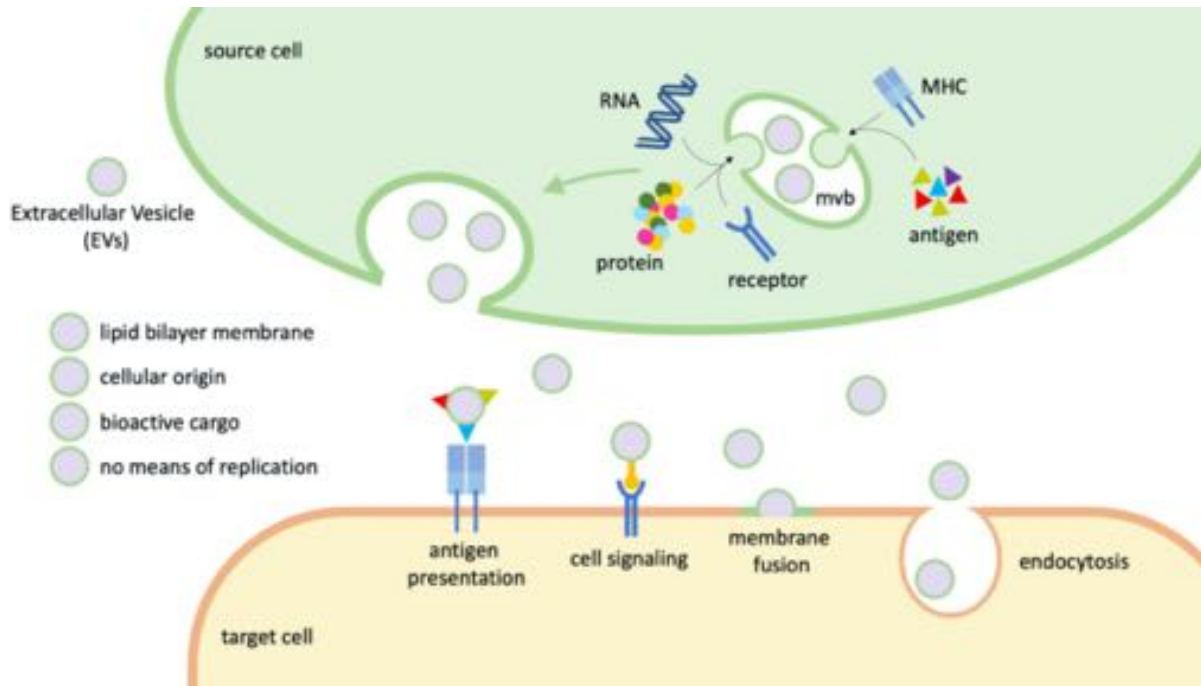


Figure 1: **EV biogenesis and interaction.** EVs encapsule bioactive cargo, such as nucleic acids, growth factor proteins, receptors, various antigens or even MHC molecules, and arise from inward budding of the multivesicular body (MVB) membrane. Upon fusion of the MVB-membrane with the cell membrane, EVs are released into the extracellular space, where they act as paracrine or even autocrine messengers. At the target cells, EVs can interact in one or more of several possible ways: 1) immunomodulatory, 2) via receptor binding and subsequent intracellular signaling cascade activation, or 3) by fusion with the plasma membrane, releasing their cargo into the cytoplasm. Additionally, EVs may be 4) internalized via different endocytotic pathways. © Maximilian Haertinger

internalization is likely dependent on the EV-producing cell and the target cell, the metabolic and signaling state of these cells, as well as the EV cargo [15, 19, 47, 51, 53, 54]. In the context of the peripheral nervous system, it has been previously shown that ASC-derived EVs are internalized by SCs, however, the internalization has not been further characterized [16]. After uptake, EVs are initially processed according to the lysosomal pathway. However, an escape from degradation is required, which is achieved by backfusion with the multivesicular endosome (MVE) membrane. The fusion leads to release of cargo into the cytosol, however, the exact mechanism of final signal transduction remains elusive [17, 19].

### 1.2.2 EVs in regenerative medicine

Due to their ubiquitous nature and involvement in various (patho-) physiological processes, EVs are promising candidates for diagnostic purposes, serving as biomarkers in liquid biopsies. Their cargo may provide insight into their cells of origin, allowing a dynamic monitoring without the need to physically remove cells for analysis [21, 55]. Prerequisite for a diagnostic EV

screening is the specific isolation of a certain EV subset. Especially immuno-selective methods have gained traction and are able to collect EVs with a consistent quantity and quality [55]. A recently developed panel of diagnostic biomarkers for disease provides a framework for cargo interpretation in disease monitoring with prognostic features [56].

In addition to diagnostic applications, EVs are attracting attention due to their regenerative capabilities and involvement in injury response. EVs of various source cells may enhance intrinsic tissue repair mechanisms. Especially vesicles derived from stem cells have been successfully used in regenerative medicine [57–61], in settings including neurodegenerative, cardiovascular, respiratory diseases, inflammation, autoimmunity and wound healing. The exact mode of regulation of EVs' influence on target cells however remains elusive and require deeper understanding to ensure a safe application and limit off-target side effects [21].

### 1.2.3 EVs in peripheral nerve regeneration

The peripheral nervous system has a limited intrinsic regenerative potential after axonal disruption, hence emerging approaches such as EVs are welcomed. EVs from both mesenchymal stem cells (MSCs) and SCs were successfully used to facilitate and enhance peripheral nerve regeneration [62, 63]. A recent study by Yu et al successfully combined SC-EVs with an artificial hydrogel nerve graft to bridge a 10 mm sciatic nerve defect in rats [64]. Additionally, potential therapeutic applications of EVs have been investigated in the central nervous system with promising results [65, 66].

## 1.3 Endocytosis

### 1.3.1 Clathrin-mediated endocytosis

The well-described process of clathrin-mediated endocytosis (CME) has been historically called receptor-mediated endocytosis (RME) due to its primary internalization cargo: transmembrane receptors with their ligands [67]. However, due to deeper understanding of endocytic events and internalization cargo, the term RME is no longer used. Upon interaction of transmembrane receptors with their respective ligands, a pioneer module that includes adaptor proteins such as the adaptor protein 2 complex (AP2) mediate translocation, nucleation and subsequent polymerization of the coat protein clathrin at the site of internalization [67]. This results in the formation of a membrane curvature that is often referred to as clathrin coated pits (CCP) [67–69]. Following clathrin polymerization, an actin filament network is assembled and aids in membrane curvature. The network includes activators such as myosin motor proteins and dynamin. To complete internalization, the the neck of the CCP is further constricted and subsequently closed. Regulated by BAR domain proteins and dynamin, the scission is completed, and eventually the clathrin coated vesicle (CCV) is uncoated by a complex of heat shock cognate 71 kDa

protein (HSC70) and auxilin [67–69].

With CCP structures ranging between 60-120 nm [68], CME is well suited for internalization of small EVs. An increasing number of studies suggests an uptake of EVs via CME in various cell types, including ovarian carcinoma cells [52, 70], cardiomyoblasts and pheochromocytoma cells [71], embryonic kidney cells [72] and macrophages [73]. As reviewed in [51], to study CME of EVs pharmacological inhibitors have been successfully used to disrupt CME at different stages: while chlorpromazine (CPZ) directly prevents CCP formation, the dynamin inhibitor dynasore prevents scission of the CCV. Additionally, dynamin, AP2 and epidermal growth factor receptor pathway substrate clone 15 (EPS15) are acclaimed targets for genetic engineering, such as knock-downs, RNAi and mutations.

### 1.3.2 Clathrin-independent endocytosis

Although responsible for a significant portion of endocytotic events, alternative clathrin-independent mechanisms are increasingly attracting interest [74]. Early studies came to the conclusion that internalization is generally dynamin dependent, however, when depleting cells of clathrin, endocytosis of certain cargoes could not be impeded [51, 52]. This suggested alternative routes of internalization, although it still was unclear whether these clathrin-independent internalization mechanisms are only compensating for the lack of clathrin. Clathrin-independent endocytosis (CIE) has since been established as discrete internalization mechanism, although crossregulation may occur [74]. Today, CIE is used as an umbrella term for several distinct pathways that are mediated by specific proteins, although, a general dependency on cholesterol can be observed. Depletion of cholesterol by methyl- $\beta$ -cyclodextrin (M $\beta$ CD) is therefore a common way to study CIE, however, cholesterol depletion may also interfere with CME and macropinocytosis (MP) [74, 75]. CIE mechanisms are further characterized based on their dependence on dynamin, a large GTPase necessary for scission of the plasma membrane to complete internalization [74, 76].

**Dynamin-dependent mechanisms.** Multiple pathways depend on dynamin for vesicle closure, the most prominent being caveolae-mediated endocytosis. Similar to CME, a variety of cargo is internalized via membrane invaginations in the presence of caveolin proteins coating the vesicles as well as sphingolipids and clustered glycosyl phosphatidylinositol-anchored proteins (GPI-APs) [67, 74, 77]. This cholesterol-dependent mechanism produces invaginations of 40-80 nm, which, after membrane scission, are further processed via the endosomal pathway. Proteins of the flotillin family have been shown to act analogous to caveolins [67]. Furthermore, an additional dynamin-dependent mechanism is known for its role in immune cells. Mediated by the small GTPase RhoA, the mechanism was first described to internalize the interleukin-2 receptor  $\beta$ -chain (IL-2R- $\beta$ ). Additional dynamin dependent mechanisms include the fast endophilin A2-dependent endocytosis (FEME), and high concentration epidermal growth factor receptor (EGFR) internalization [67, 74].

**Dynamin-independent mechanisms.** Internalization may also occur independent of clathrin and dynamin, and share the use of small GTPases. CDC42, a small GTPase of the Rho family, plays a major role in the internalization of GPI-APs and produces rather different membrane structures compared to spherical invaginations of other CME and CIE events [67, 74, 77]. A notable volume is internalized via wide elongations, coregulated by sorting nexin 9 (SNX9). This CDC42 dependent internalization is also referred to as clathrin-independent carrier/glycosylphosphatidylinositol (GPI)-anchored protein-enriched endosomal compartments, short CLIC/GEEC [74, 76, 78].

### 1.3.3 Macropinocytosis

While the majority of both CME and CIE result in small endosomal vesicles, MP is a process of large volume internalization by fusion of plasma membrane protrusions engulfing fluid phase volumes, creating irregular shaped macropinosomes. While only a set of specialized cells are proficient of constitutive MP, it can be stimulated by growth factors such as epidermal growth factor (EGF) and platelet-derived growth factor (PDGF) [79]. MP requires extensive cytoskeletal remodeling known as membrane ruffling and is therefore dependent on actin and PI3-kinase [79]. In MP regulation, sorting nexins play a central role and are located at macropinosomes. By binding to and thereby activating rac1, p21-activated kinase 1 (PAK1) has been shown to be sufficient to induce MP [80]. A comprehensive characterization of MP regulation has not yet been achieved, known regulators are reviewed by Lim et al [79].

After backfolding of lamellipodia, macropinosomes can be closed either dynamin-dependent or dynamin-independent [74]. Upon internalization, macropinosomes are depleted of endocytosis markers and acquire endosomal markers such as Rab7 in a process called macropinosomal maturation. Ultimately, macropinosomes are fused with lysosomes for final processing. Although maturation occurs in all cells capable of MP, its regulation is cell type specific [79].

Due to its cytoskeletal remodeling, MP is found in close relationship with cell motility. This relationship however can be hijacked during tumor progression and metastasis. Additionally, antigen presenting cells such as dendritic cells and macrophages constantly probe their surroundings via MP, internalizing peptides that are further loaded onto MHC molecules and presented to T cells [79, 81].

## 1.4 Rationale and importance of this study

The number of potential applications grows together with the body of knowledge around EV biology. However, there are still too many unknowns for a safe application in humans. As reviewed by Margolis and Sadovsky [17], there are at least eight aspects that require more insight. First, the heterogenous size distribution of EVs and its implications for their function are poorly understood. The second consideration evolves around the biogenesis pathway and

the resulting membrane composition. Furthermore, not only the vesicles themselves but also their cargo require further investigation, especially regarding redundancies and intercargo relationships. How EVs manage a specific interaction with target cells remains unanswered, as does the involvement of EVs in viral transmission.

This study aims at answering the first part of the sixth open question: EV entry, unpacking and subsequent cargo processing, within the scope of peripheral nerve regeneration. Following PNI, SCs are the main drivers of regeneration, paving the way to successful reinnervation. Hence, the interaction between SCs and ASC-EVs was investigated. Initially, the temperature sensitivity and energy dependency was established. Modes of internalization were investigated by selectively inhibiting the most common routes of EV internalization, CME and MP. With imaging flow cytometry, this investigation combined high throughput with spatial resolution, which allowed analysis on a single cell level.

## 2 Methods

### 2.1 Animals

Nerves (*N. ischiadicus*) and intraabdominal adipose tissue was harvested from adult male Lewis rats aged 12 to 16 weeks old following decapitation under isoflurane anesthesia. While sciatic nerve tissue was excised from wildtype Lewis rat cadavers, adipose tissue was harvested from the transgenic strain LEW-Tg(CAG-EGFP)1Ys as well. Sacrifice of the animal and tissue harvest was performed in accordance with the Austrian Animal Testing Law (TVG 2012, §2, 1.c) and the Directive 2010/63/EU of the European Parliament and of the Council.

### 2.2 Schwann cells

#### 2.2.1 Schwann cell isolation and culture

Primary rat Schwann cells were isolated, cultured and enriched according to the protocol established by Weiss et al. [82] with previously described adaptations [11, 16]. In brief, following initial mechanical dissection nerve fascicles were enzymatically digested overnight at 37°C with 5% CO<sub>2</sub>, with MEM $\alpha$  (GlutaMAX™-1, GIBCO, Waltham, MA, USA) supplemented with 1% penicillin-streptomycin (P/S, GIBCO), 2.5% 4-(2-hydroxyethyl)-1-piperazineethanesulfonic acid (HEPES, GIBCO), 1% sodium pyruvate (GIBCO), 10% fetal calf serum (FCS, LINARIS, Dossenheim, Germany), 0.125% (w/v) collagenase type IV (GIBCO), 1.25 U/ml dispase II (Sigma-Aldrich, St. Louis, MO, USA) and 3 mM calcium chloride (CaCl<sub>2</sub>, Merck Millipore Ltd., Tullagreen, IRL).

The digestion solution was seeded on cell culture dishes coated with 0.01% poly-L-lysine hydrobromide (PLL, Sigma-Aldrich) and 5 µg/ml laminin (Sigma-Aldrich) to improve cell adhesion. SCs were cultured with Schwann cell expansion medium (SCEM) consisting of MEM $\alpha$  (GIBCO) supplemented with 2.5% HEPES (GIBCO), 1% penicillin-streptomycin (P/S, GIBCO), 1% sodium pyruvate (GIBCO), 5% (FCS, LINARIS, Dossenheim, Germany), 10 ng/mL recombinant heregulin $\beta$ -1 (PeproTech, London, UK), 0.5% N-2 supplement (GIBCO), 2 µM forskolin (Sigma-Aldrich), 10 ng/mL recombinant FGF basic (PeproTech), and 5 ng/mL PDGFAA (PeproTech). Cell culture dishes for SCs were coated as mentioned above. By exploiting specific adhesion properties, SC cultures were enriched as previously described [82].

## 2.2.2 Schwann cell characterization

SCs were seeded on PLL/laminin coated 8-well  $\mu$ -slides (Ibidi, Grafelfing, Germany) at a seeding density of 8,000 cells per cm<sup>2</sup> and cultured in SCEM for 24 - 48 h. Cells were fixed with 4.5% formaldehyde for 15 min, immunofluorescence staining was performed as previously described in Haertinger, Weiss, Mann et al. [16]. Briefly, unspecific reactive sites were blocked with 3% goat serum (DAKO, Agilent, Santa Clara, CA, USA) and 1% BSA for 20 min. Primary antibodies were incubated over night at 4°C, whereas secondary conjugated antibodies were incubated for 1 h at RT. Antibodies were applied in 1  $\times$  PBS supplemented with 1% BSA and 1% goat serum. Antibodies are listed in table 1. Nuclei were stained with 50 µg/mL 4,6-diamidino-2-phenylindole solution (DAPI, Thermo Fisher Scientific) for 10 min. To prolong storage times and reduce photobleaching, stained cells were mounted with Fluoromount-G™ mounting medium (Invitrogen).

## 2.3 Adipose tissue derived stem cells

### 2.3.1 Adipose tissue derived stem cell isolation and culture

To obtain primary adipose tissue derived stem cells, intraabdominal adipose tissue was excised, washed with 1  $\times$  PBS (GIBCO) containing 1% P/S, and minced prior to enzymatic digestion with 1 mg/ml collagenase type CLS (type 1, Merck, Darmstadt, Germany) for 1 h at 37°C. The digest was filtered through a 70 µm nylon cell strainer (FALCON, Corning Inc., Corning, NY, USA) prior to pelleting with 300  $\times$ g for 7 min. The pellet was washed with HBSS (Lonza Group Ltd, Basel, Switzerland) containing 0.5% bovine serum albumin (BSA, Sigma-Aldrich) before another centrifugation step at 300  $\times$ g for 5 min. ASCs were then seeded and cultured in growth medium based on Dulbecco's Modified Eagle Medium (DMEM) + GlutaMAX™-I with 4.5 g/l D-glucose (DMEM-HG, GIBCO) supplemented with 10% FCS, 1% P/S and 2 ng/ml recombinant human FGF basic. ASC cultures were characterized via flow cytometry to assess purity and expression of established markers.

Table 1: **Primary and secondary antibodies.**

Species: ch... chicken, gt... goat, h... human, m... mouse, r... rat, rb... rabbit

Applications: FC... flow cytometry, IF... immunofluorescence, IFC... imaging flow cytometry

antigen	species	host	clone/lot	company	application	conjugate	concentration
CD29	m/r	-	REA1074	Miltenyi	FC	PE	1:50
CD63	r	-	REA444	Miltenyi	FC, IFC	APC	1:50
CD81	m/r	-	EAT2	Miltenyi	IFC	VioBlue®	1:50
CD90.1	m/r	-	REA838	Miltenyi	FC	VioBlue®	1:50
p75NTR XP®	h/m/r	rb	D4B3/8238S	Cell Signaling	IF	-	1:400
Sox10	h	m	A-2	Santa Cruz	IF	-	1:100
S100	h	rb	GA504	Agilent - Dako	IF	-	1:200
THY1	r	m	OX7	Santa Cruz	IF	-	1:100
Vimentin	h/m/r	ch	PA1-16759	invitrogen	IF	-	1:300
anti-mouse IgG (H+L)	m	gt	A-11001	invitrogen	IF	AlexaFluor® 488	1:300
anti-rabbit IgG (H+L)	rb	gt	A32731	invitrogen	IF	AlexaFluor® 488P	1:600
anti-rabbit IgG (H+L)	rb	gt	1844440	invitrogen	IF	AlexaFluor® 594	1:500
anti-mouse IgG (H+L)	m	gt	A-21236	invitrogen	IF	AlexaFluor® 647	1:400
anti-chicken IgY (H+L)	ch	gt	SA5-10073	invitrogen	IF	DyLight® 650	1:400

### 2.3.2 Adipose tissue derived stem cell characterization

**Multilineage differentiation potential.** Adipogenic and osteogenic differentiation potential was assayed by culturing ASCs with differentiation medium (PromoCell, Heidelberg, Germany) according to the manufacturers instructions. To test for chondrogenic differentiation potential,  $2.5 \times 10^4$  ASCs per well were pelleted in Lipidure® (NOF CORPORATION Life Science Products Div., Tokyo, Japan) coated 96-well U-bottom microplate (Greiner Bio-One International GmbH, Kremsmuenster, Austria) at  $300 \times g$  for 5 min. ASCs were cultured with chondrogenic differentiation media based on DMEM-HG supplemented with 10% FCS, 1% P/S, 1% sodium pyruvate, 100 mM dexamethason (Sigma-Aldrich), 50 ng/ml ascorbic acid (Sigma-Aldrich) and 10 ng/ml recombinant TGF- $\beta$  (PreproTech). Differentiation media was changed three times per week. After 20 days in culture, cells were fixed with 4.5% formaldehyde (SAV Liquid Production GmbH, Flintsbach am Inn, Germany) for 15 min, followed by washes with  $1 \times$  PBS prior to subsequent staining. To confirm adipogenic differentiation, cells were stained with Oil Red O and counterstained with hematoxylin (Merck). Osteogenic differentiation was analyzed via alizarin red staining. Furthermore, chondrogenic cell pellets were stained with alcian blue to visualize glycosaminoglycan deposition.

**Immunophenotyping.** ASC cultures were characterized by assessing the expression of established cell surface antigens. Following cell harvested, immunostaining was performed at 4°C in flow buffer consisting of  $1 \times$  PBS supplemented with 0.5% BSA, 2 mM ethylenediaminetetraacetic acid (EDTA, Sigma-Aldrich) and 1% sodium azide ( $\text{NaN}_3$ , Merck). Antibodies are listed in table 1. For immunostaining with conjugated primary antibodies, cells were incubated with

respective antibodies for 20 min, followed by two washes with flow buffer (5 min, 300×g). Unconjugated primary antibodies were added to the cell suspension for 30 min before two washes with flow buffer (5 min, 300×g) and subsequent detection of primary antibodies with conjugated secondary antibodies for 30 min. Stained cells were washed thoroughly prior to flow cytometric analysis with FACSCanto™-II (Becton, Dickinson and Company, Franklin Lakes, USA). Flow cytometry data was processed with Kaluza 2.1 analysis software (Beckman Coulter GmbH, Krefeld, Germany).

## 2.4 Adipose tissue derived stem cell extracellular vesicles

### 2.4.1 Adipose tissue derived stem cell extracellular vesicle isolation

Prior to isolation of EVs, 60 - 70% confluent ASCs in passage 2 to 4 were conditioned with serum-free growth medium for 24 h. Conditioned ASC culture supernatant was centrifuged at 300×g for 10 min at 4°C. The supernatant was transferred into a new tube and subjected to a secondary centrifugation step (2,000×g for 20 min at 4°C) prior to being filtered through a 0.22 µm filter unit with Durapore® PVDF membrane (Merck). To enrich EVs by sequential ultracentrifugation, the filtered supernatant was transferred into ultracentrifugation tubes and centrifuged at 100,000×g for 90 min at 4°C with a fixed angle rotor (T-865;  $k\text{-factor}_{max} = 51.7$ ; Thermo Fisher Scientific Inc., Waltham, MA, USA). The resulting supernatant was discarded, whereas the pellet was resuspended in 20 ml 1×PBS without  $\text{Ca}^{2+}\text{Mg}^{2+}$ . EVs were further enriched by a second ultracentrifugation step at 100,000×g for 90 min at 4°C. The EV pellet was then resuspended in 100 µl 1×PBS without  $\text{Ca}^{2+}\text{Mg}^{2+}$ , transferred into protein low-binding tubes (Eppendorf AG, Hamburg, Germany) and stored at -80°C until further use.

### 2.4.2 Adipose tissue derived stem cell extracellular vesicle characterization

**Size distribution and concentration estimation** To establish size distribution of isolated vesicles, aliquots of the resuspended ultracentrifugation pellet were diluted 1:7,500 with 1×PBS prior to analysis with Zetaview (Particle Metrix GmbH, Inning am Ammersee, Germany). Size distribution was measured in scatter mode with camera settings as follows: sensitivity 70, shutter 50, frame rate 30. 11 positions were measured in three cycles, analysis parameters were set to max area 1,000, min area 10, brightness 30.

**Immunophenotyping** ASC-EVs were tested for tetraspanins CD63 and CD81 by immunofluorescence staining and subsequent analysis via imaging flow cytometry. To prevent antibody aggregation that could potentially distort small particle analysis, fluorescently labeled antibodies were centrifuged at 18,000×g for 5 min at 4°C and only the supernatant was used for

further staining. EVs in 1×PBS were stained for 60 min at RT. Antibodies were diluted 1:50 with 1×PBS, CellMask™ Green plasma membrane stain (Invitrogen, Waltham, MA, USA) was used at a dilution of 1:500. Following the incubation period, the EVs in staining solution were diluted 15× with 1×PBS. Antibodies are listed in supplementary table ???. Imaging flow cytometry was performed with Amnis ImageStream<sup>X</sup>-MkII (Amnis, Proteigene, Saint Marcel, France) and IDEAS™v6.2 software (Amnis). Laser settings were as follows: 405 nm at 120 mW, 488 nm at 150 mW, 561 nm at 150 mW, 642 nm at 150 mW and SSC at 1 mW; images were acquired at 60× magnification. For increased resolution, sampling was performed at low speed, high sensitivity. In figure 6A, the gating strategy applied to analyze the ASC-EVs is shown. As the ImageStream<sup>X</sup> system uses calibration beads, an initial discrimination between beads and vesicles was performed based on the scatter (figure 6A1) and membrane dye CMG (figure 6A2). To confirm that beads and vesicles can be discriminated based on CMG intensity (figure 6A2), CMG<sup>+</sup> and CMG<sup>-</sup> populations were analyzed separately for their scatters signal intensity. Within the *beads* gate, events could only be found within the CMG<sup>-</sup> population (figure 6A4), and vice versa (figure 6A3).

## 2.5 ASC-EV internalization assay

### 2.5.1 Fluorescent labeling of ASC-EVs

To enable localization analysis, EVs were stained with the membrane dye PKH67 (Sigma-Aldrich). To this end, thawed EVs were concentrated with Amicon® ultrafiltration tubes (10 kDa molecular weight cut off, Merck) at 3,000×g for 20 min. Staining was achieved with a dye concentration of 4 μM. Following 5 min incubation at RT, staining was stopped with SCEM. To remove excess dye, EVs in staining solution were transferred to Amicon® ultrafiltration tubes (10 kDa molecular weight cut off, Merck) and centrifuged at 3,000×g for 20 min.

### 2.5.2 Internalization verification and nuclear translocation

SCs were seeded on PLL/laminin coated 8-well μ-slides (Ibidi, Grafelfing, Germany) until 70% confluence and incubated with EVs for up to 2 hours. Cells were fixed with 4.5% formaldehyde for 15 min, immunofluorescence staining was performed as previously described in Haertinger, Weiss, Mann et al. [16]. Briefly, unspecific reactive sites were blocked with 3% goat serum (DAKO, Agilent, Santa Clara, CA, USA) and 1% BSA for 20 min. Primary antibodies were incubated over night at 4 °C, whereas secondary conjugated antibodies were incubated for 1 h at RT. Antibodies were applied in 1×PBS supplemented with 1% BSA and 1% goat serum. Antibodies are listed in table 1. Nuclei were stained with 50 μg/mL 4,6-diamidino-2-phenylindole solution (DAPI, Thermo Fisher Scientific) for 10 min. To prolong storage times and reduce photobleaching, stained cells were mounted with Fluoromount-G™ mounting medium (Invitrogen). High resolution confocal micrographs were obtained with an LSM780 equipped with Airyscan

(Carl Zeiss Microscopy GmbH, Jena, Germany). Images were processed in ZEN 2 acquisition software provided by Carl Zeiss Microscopy GmbH.

### 2.5.3 Visualization of early-stage ASC-EV internalization

SCs were seeded on PLL/laminin coated Aclar discs and cultured until 70% confluence and incubated with EVs up to 4 h at 37 °C. Cell cultures were fixed with 2.5% EM grade glutaraldehyde solution for 1 h. After fixation, cells were washed with 0.1 M cacodylate buffer and subsequently stained with 1% osmium tetroxide ( $\text{OsO}_4$ , Electron Microscopy Sciences) and 1.5% potassium ferrocyanide ( $\text{K}_4[\text{Fe}(\text{CN})_6]$ , Merck) for 2 h at RT. SCs were dehydrated with ethanol (10 min each at RT on shaker: 30%, 50%, 70%, 80%, 2×96%, 3×100%). Infiltration and embedding was performed based on a protocol provided by the Electron Microscopy Facility at Vienna BioCenter Core Facilities (VBCF), member of the Vienna BioCenter (VBC), Austria. In the initial infiltration step, fixed and osmium-macerated cells were incubated with one volume epoxy resin (44.15% epoxy embedding medium (1,2,3-propanetriol glycidyl ether, SERVA Electrophoresis GmbH), 35.32% 2-dodecenylsuccinic anhydride (DDSA, SERVA Electrophoresis GmbH), 17.66% methyl nadic anhydride (MNA, SERVA Electrophoresis GmbH), 2.87% benzyldimethylamine (BDMA, SERVA Electrophoresis GmbH)) and two volumes 100% ethanol for 30 min at RT. The infiltration medium was replaced with equal parts epoxy resin and 100% ethanol, which again after 30 min were replaced with two parts epoxy resin, one part 100% ethanol. Lastly, cells were infiltrated twice with epoxy resin for 30 min at RT prior to embedding in epoxy resin. The resin was hardened at 60 °C for 48 hours. Ultrathin (70 nm) sectioning, uranyl acetate contrasting and imaging of embedded SCs was performed by the Electron Microscopy Facility at Vienna BioCenter Core Facilities (VBCF), member of the Vienna BioCenter (VBC), Austria.

### 2.5.4 Establishing energy-dependency of ASC-internalization

SCs were seeded on PLL/laminin coated borosilicate glass coverslips (Paul Marienfeld GmbH & Co.KG, Lauda Konigshofen, Germany), cultured until 70% confluence and pretreated with 100 mM sodium azide for 30 min at 37 °C, or pre-cooled at 4 °C for 30 min before incubation with EVs at either 4 °C or 37 °C for 30 min, respectively. Cell cultures were fixed with 2.5% EM grade glutaraldehyde solution (Sigma-Aldrich) and following thorough washing, dehydrated with ascending concentrations of ethanol (10 min each at RT on shaker: 30%, 50%, 70%, 80%, 2×96%, 3×100%). After drying by evaporation of hexamethyldisilazane (HMDS, Sigma-Aldrich), samples were sputter coated with 12 nm gold. Micrographs were obtained with a FEI Feg 250™ (FEI Company, Hillsboro, OR, USA) in high vacuum with secondary electron detector at 15 kV.

### 2.5.5 Inhibitor cytotoxicity

To account for cytotoxic effects of inhibitors and their solvents, MTT-based CellTiter 96<sup>®</sup> non-radioactive cell proliferation assay (Promega GmbH, Waldorf, Germany) was performed. Following manufacturers instructions, SCs seeded in PLL/laminin coated 48-well microplates (Greiner Bio-One International GmbH) with 10,000 cells per cm<sup>2</sup> and cultured in SCEM without inhibitors. After 48 hours, SCs were washed twice with 1×PBS prior to inhibitor treatment. Growth medium controls as well as solvent controls were included. SCs were treated with inhibitors for 3 h at 37°C. The viability assay was performed as per the manufacturers instructions. To determine tetrazolium conversion, absorption was measured at 570 nm with reference wavelength of 650 nm. Absorbance values were corrected with respective absorbance measurements of solvent controls. The cytotoxicity assay was performed in six biological replicates (n=6).

### 2.5.6 Endocytosis inhibitor treatment

SCs were seeded in PLL/laminin coated 12-well plates at 10,000 cells per cm<sup>2</sup> and cultured in serum-free SCEM until 90% confluent. Upon reaching desired cell density, SCs were pre-treated for 30 min with 10 - 100 µM EIPA, 5 - 25 µM CPZ, or 1 - 10 mM MβCD. After 30 min, PKH67-labeled EVs (0.8×supernatant of one T175 flask per well) were added for 3 h and subsequently external EVs and inhibitors removed by washing with 1×PBS. SCs were detached with 0.25% trypsin-EDTA and immediately cooled until imaging flow cytometry analysis. The EV internalization inhibition assay was performed in three biological replicates (n=3).

### 2.5.7 ASC-EV internalization assessment via imaging flow cytometry

Following internalization assays, SCs were washed with 1×PBS and harvested with StemPro™ Accutase™ cell dissociation reagent (GIBCO) and pelleted with 300×g for 5 min. SCs were re-suspended in flow buffer without BSA for analysis. Imaging flow cytometry was performed with Amnis ImageStream<sup>X</sup>-MkII (Amnis, Proteigene, Saint Marcel, France) and IDEAS™ v6.2 software (Amnis). The 488 nm laser was set to 20 mW, images were obtained at 60× magnification. For increased resolution, sampling was performed at low speed, high sensitivity.

To quantify the internalization of EVs, imaging flow cytometry was employed. First, cells in focus were identified with the *Gradient RMS* feature based on the brightfield images (see figure 2 A1). Here, sharpness quality is assessed based on large variations of intensity levels. Similar to flow cytometry, single cells were identified, but due to the lack of forward scatter the gating was performed on an area vs. aspect ratio scatter plot, as shown in figure 2 A2. For internalization analysis, events with a positive PKH67 signal were gated on a scatter plot of the intensity features *Max Pixel* and *Intensity* (see figure 2 A3). Further, a mask was based on the brightfield image (Ch01) and eroded with the *AdaptiveErode* feature, with the erosion coefficient set at 95. Using the internalization wizard, an internalization score was determined by calculation of a

ratio of EVs inside the eroded cell mask or outside. Additionally, the feature *Spot Count* was used to determine the amount of internalized EVs. To enable automated analysis, positive and negative truth populations of at least 25 cells were assigned.

## 2.6 Statistical analysis

Acquired data was statistically analyzed with GraphPad Prism 9. Unless stated otherwise, data are presented as mean  $\pm$  standard deviation. For inhibitor cytotoxicity tests, replicates were averaged and mean values normalized to untreated controls. Internalization of ASC-EVs by inhibitor treated SCs was assessed with three parameters, PKH positivity, internalization score and spot count. For all parameters, replicate values were averaged and mean values were normalized to untreated controls, and presented as fractions of untreated controls. A two way ANOVA with Dunnet's multiple comparisons test was performed with normalized mean values. A p-value  $<0.05$  was considered significant.

# 3 Results

## 3.1 Characterization of SCs, ASCs and ASC-EVs

### 3.1.1 Characterization of SCs

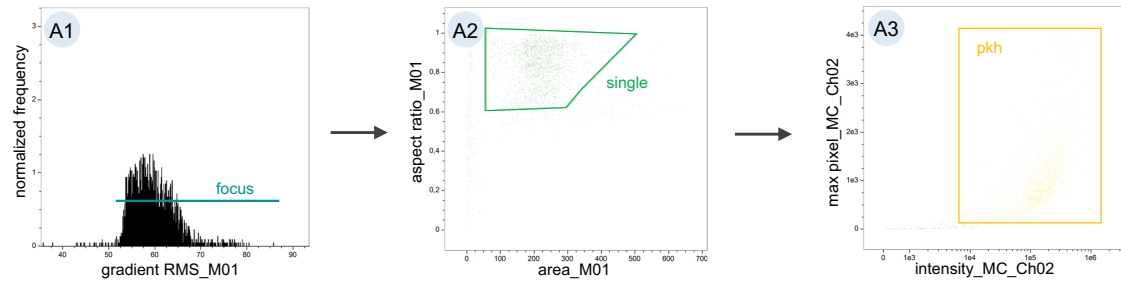
SCs were isolated from sciatic nerves and cultured in PLL/laminin coated tissue culture hardware. Initially, SCs in p0 showed bi- and multipolar processes, however, at p3 onwards typical spindle shaped morphology and alignment could be observed. To confirm expression of characteristic marker proteins, immunofluorescence stainings were performed and are presented in figure 3. SCs showed strong expression of low affinity nerve growth factor receptor (NGFR) (figure 3A2), although lack the expression of THY1, a commonly used fibroblast marker glycoprotein (see figure 3A3). Moreover, the expression of calcium shuttle protein S100 (figure 3B2) and glial transcription factor Sox10 (figure 3B5) could be confirmed, in addition to intermediate filament vimenting (figure 3B3).

### 3.1.2 Characterization of ASCs

Adipose stem cells (ASCs) were isolated from intra-abdominal adipose tissue and expanded to serve as source cells for EVs. ASCs were plastic-adherent and showed characteristic morphology (figure 4B1). ASC cultures were further characterized by their expression of marker

## Imaging Flow Cytometric Analysis

### A Gating Strategy



### B Internalization Analysis

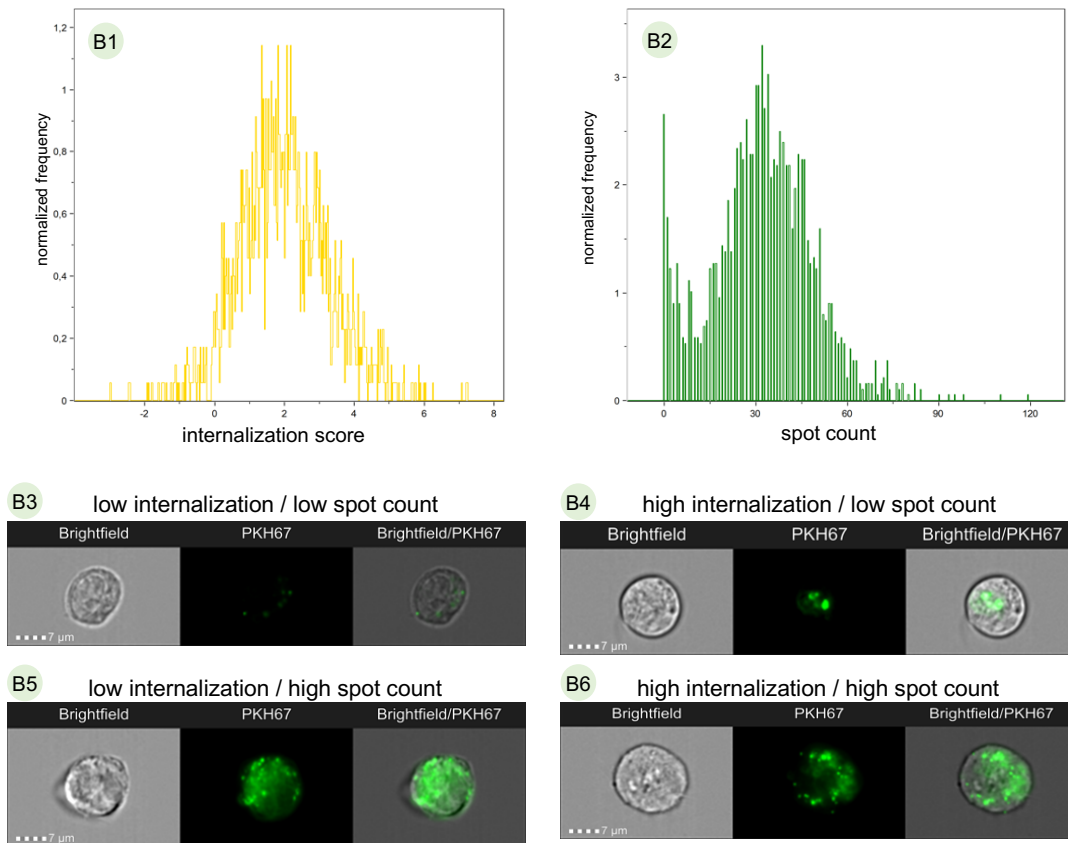


Figure 2: **Imaging flow cytometric analysis.** **A)** Gating strategy to determine EV internalization. First, cells in focus (**A1**) were identified and further gated to find single cells (**A2**) and cells with PKH67 signal (**A3**). **B)** EV-internalization quantification by internalization score (**B1**) and spot count inside the cell (**B2**). Multiple subpopulations were identified: SCs with low internalization score and low spot count (**B3**), high internalization score but low spot count (**B4**), low internalization score with high spot count (**B5**), and both high internalization score and high spot count (**B6**).

### Characterization of SCs

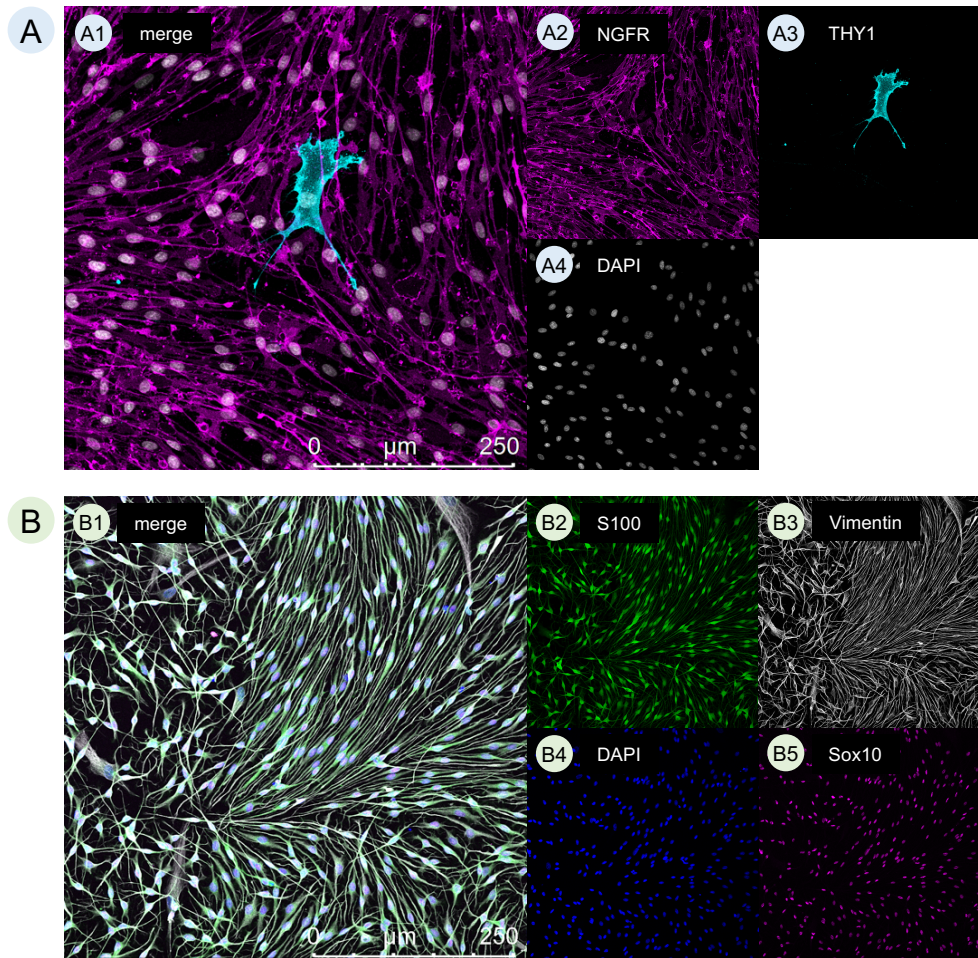


Figure 3: **Characterization of SCs.** **A)** Immunofluorescence staining of SCs with merged channels (**A1**) and single channels of NGFR (**A2**), THY1 (**A3**) and DAPI (**A4**). **B)** Immunofluorescence staining of SCs with merged channels (**B1**) and single channels of S100 (**B2**), Vimentin (**B3**), DAPI (**B4**) and Sox10 (**B5**).

antigens CD29, CD63 and CD90 via flow cytometry, a representative scatter plot (FSC-A vs. SSC-A) can be found in supplementary figure 4A1. While CD29 (figure 4A2) and CD63 (figure 4A3) were comparably abundant in all ASC cultures, CD90 expression was inconsistent, as shown in figure 4A4. Further, the multilineage differentiation potential of ASCs was assessed. Adipogenic differentiation potential was confirmed with oil red o staining of lipid vacuoles (figure 4B2), osteogenic differentiation potential was confirmed by staining of extracellular calcium deposits (figure 4B3). Chondrogenic differentiation potential of pelleted ASCs was confirmed with alcian blue staining of extracellular matrix collagen (figure 4B4).

### 3.1.3 Characterization of ASC-EVs.

After a 24 hour serum-free conditioning period, the supernatant of ASC cultures up to passage 4 was harvested, and ASC-derived small EVs were isolated via differential ultracentrifugation, as schematically depicted in figure 5A, and stored at -80 °C. Size distribution of thawed EVs was established with NTA, representatively shown in figure 5B. A Gaussian curve was further fitted to the size distribution with an  $R^2$  of 0.9158. The mean size of particles was thereby determined at  $124.3 \pm 39.98$  nm. The expression of tetraspanins CD63 and CD81 was demonstrated via immunophenotyping (figure 5C, D). Additionally, the lipid bilayer membrane was stained with

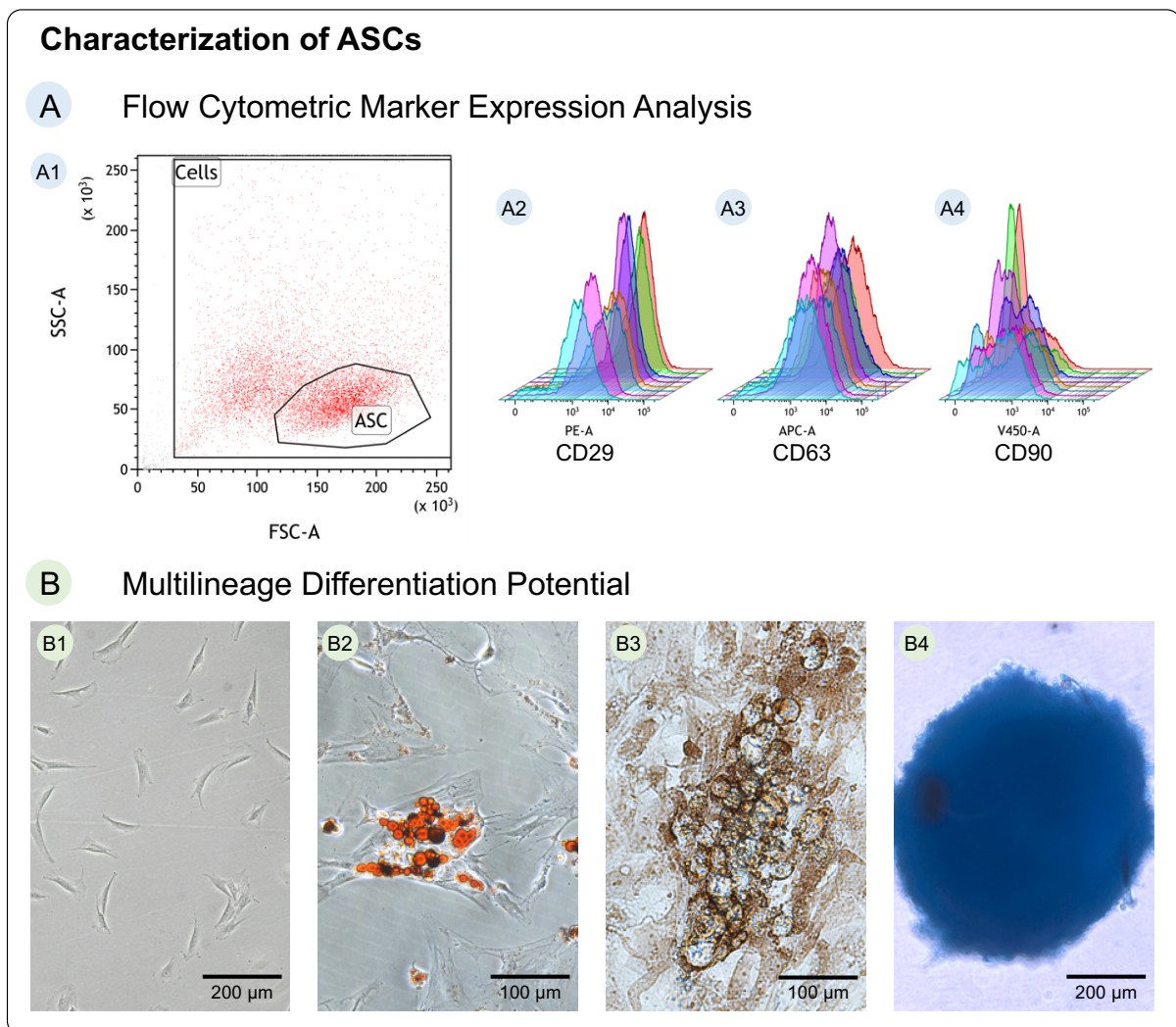


Figure 4: **Characterization of ASCs.** **A)** Using flow cytometry, marker expression was analyzed. Representative scatter plot (**A1**) and overlay of 8 individual ASC cultures analyzed for their expression of CD29 (**A2**), CD63 (**A3**) and CD90 (**A4**). **B)** Multilineage differentiation potential of primary ASCs. Undifferentiated ASCs in passage 2 (**B1**), adipogenically differentiated ASCs stained with oil red o (**B2**), osteogenically differentiated ASCs stained with alizarin red (**B3**) and chondrogenically differentiated ASCs stained with alcian blue (**B4**).

CMG. This staining was used to discriminate between calibration beads and ASC-EVs. The CMG<sup>+</sup>/scatter<sup>-</sup> ASC-EVs (figure 6A3) and CMG<sup>-</sup>/scatter<sup>+</sup> calibration beads (figure 6A4) were thereby identified in a scatter plot (figure 6A5). This approach was further confirmed with a lysis control, where EVs were lysed with RIPA buffer (Thermo Fisher Scientific) for 30 min at RT prior to staining. While CMG<sup>-</sup>/scatter<sup>+</sup> calibration beads could still be identified, CMG<sup>+</sup>/scatter<sup>-</sup> ASC-EVs were no longer present in the lysis control (figure 6A6).

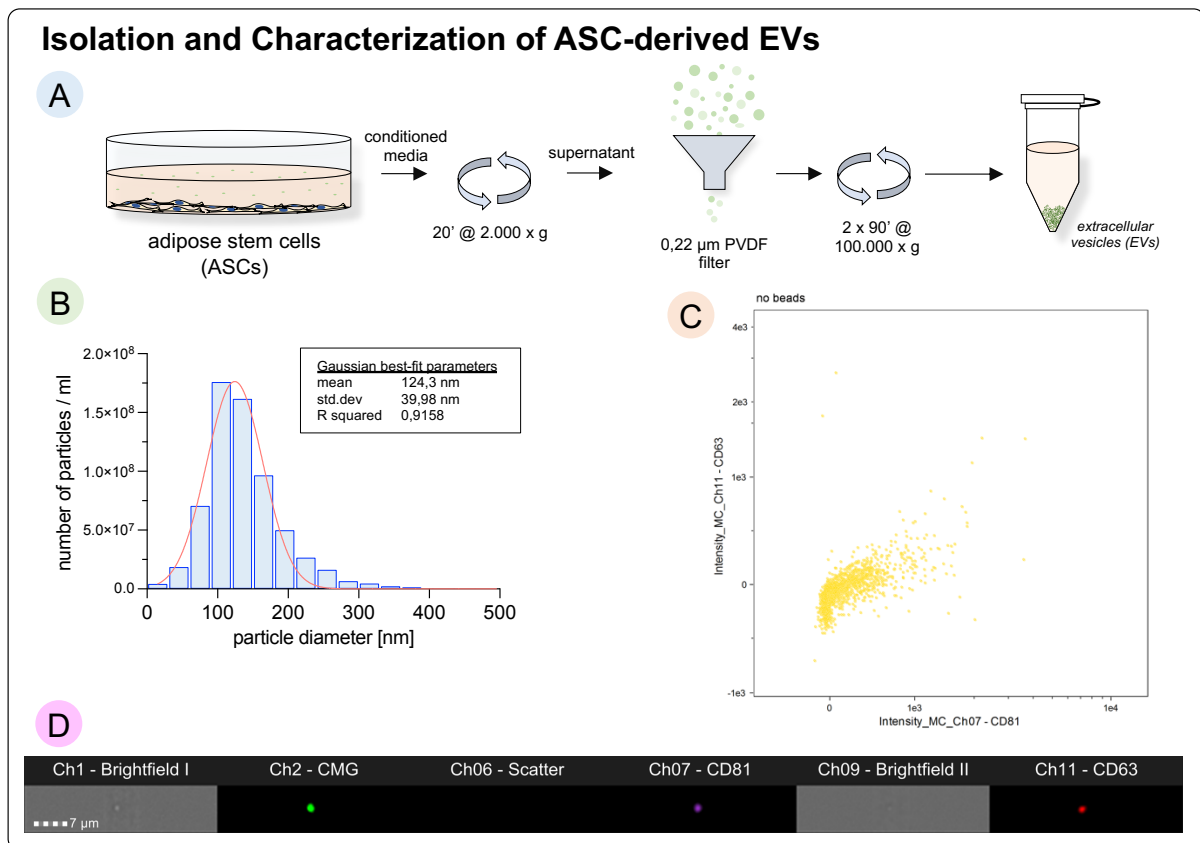
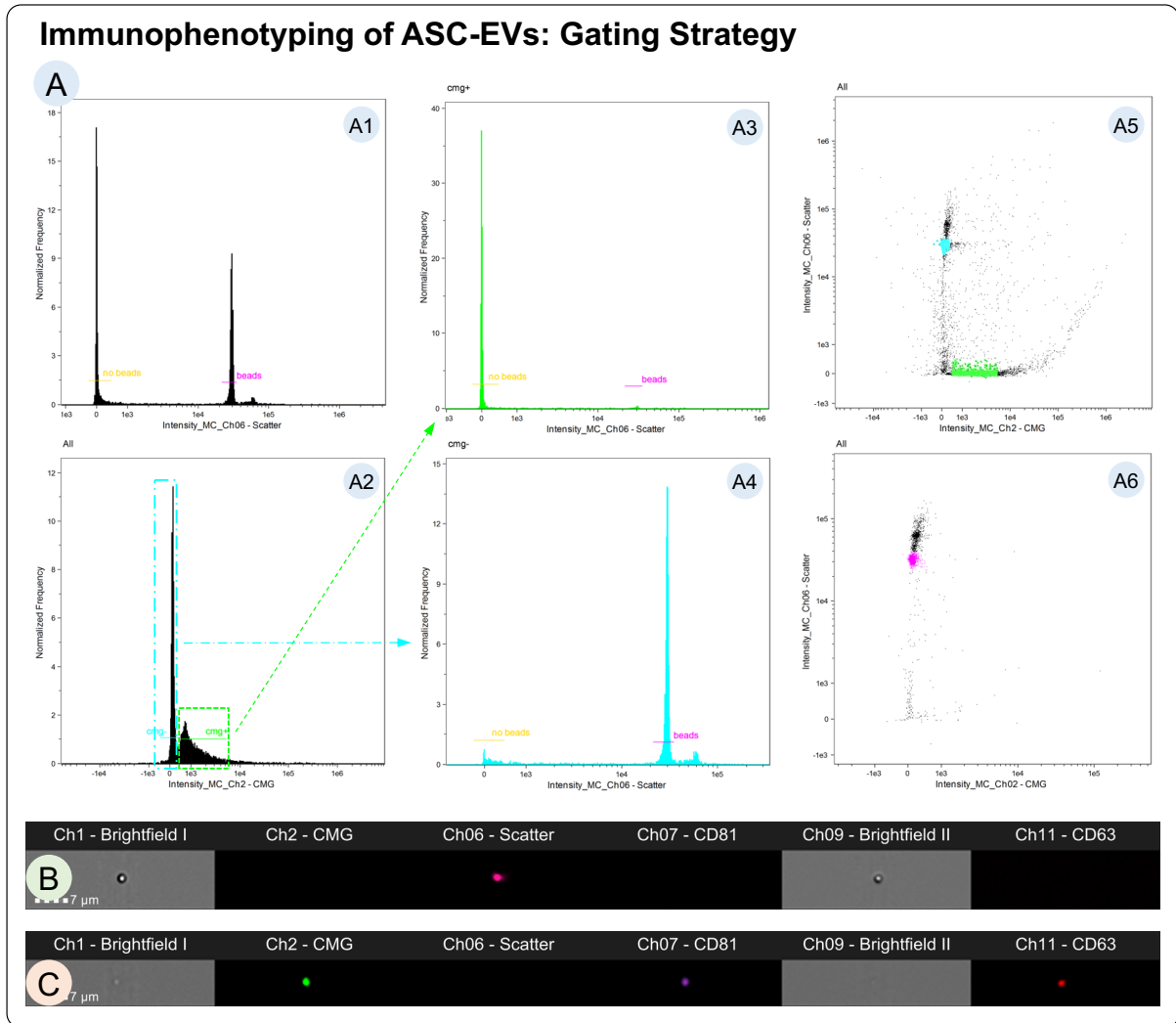


Figure 5: **Characterization of ASC-EVs.** **A)** Schematic depiction of EV isolation process. **B)** Size distribution histogram of EVs as established with nanoparticle tracking analysis. **C)** Immunophenotyping of ASC-EVs. Expression analysis scatter plot of tetraspanins CD63 vs. CD81. **D)** Exemplary imagestream gallery of triple positive ASC-EV: CMG, CD81 and CD63.

### 3.2 Internalization of ASC-EVs by SCs

To assess the interaction with ASC-EVs, SCs were treated with lipophilic membrane dye PKH67 labeled EVs for up to 3 hours prior to fixation and membranous immunofluorescence staining of SCs using the tumor necrosis factor receptor superfamily member 16 (NGFR) characteristically expressed by cultured SCs. Volumetric reconstruction of confocal z-stacks showed that EVs are located inside the SCs cytoplasm localized in a perinuclear pattern (figure 7A). PKH67<sup>+</sup> signals were observed in small size ranges (<200 nm) as well as larger signal aggregates (figure 7A2)

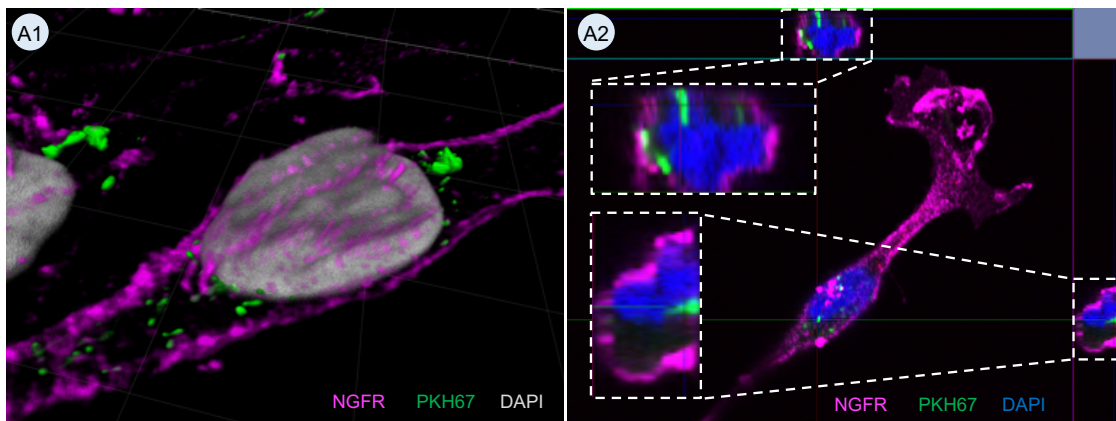


**Figure 6: Immunophenotyping of ASC-EVs: Gating Strategy.** **A)** Gating strategy to discriminate between calibration beads and vesicles. **B)** Exemplary image of calibration bead. **C)** Exemplary image of ASC-EV positive for CMG, CD81 and CD63.

up to 2 μm. Smaller signals were identified mostly in the cellular periphery, while larger signal aggregates were located close to the nucleus, suggesting perinuclear accumulation. Transmission electron micrographs enabled an in-depth investigation of the structures involved in the initial translocation of internalized EVs. To this end, SCs were treated with ASC-EVs for 30 min prior to fixation. Bilayer delimited vesicular structures with diameters around 120 nm were observed in the SCs' processes. These vesicles were found near cytoskeletal filaments (figure 7B1, B2) or inside a lumen (figure 7B3, B4), indicating more than one mode of internalization.

## Internalization of ASC-EVs in SCs

### A Confocal Microscopy



### B Transmission Electron Microscopy

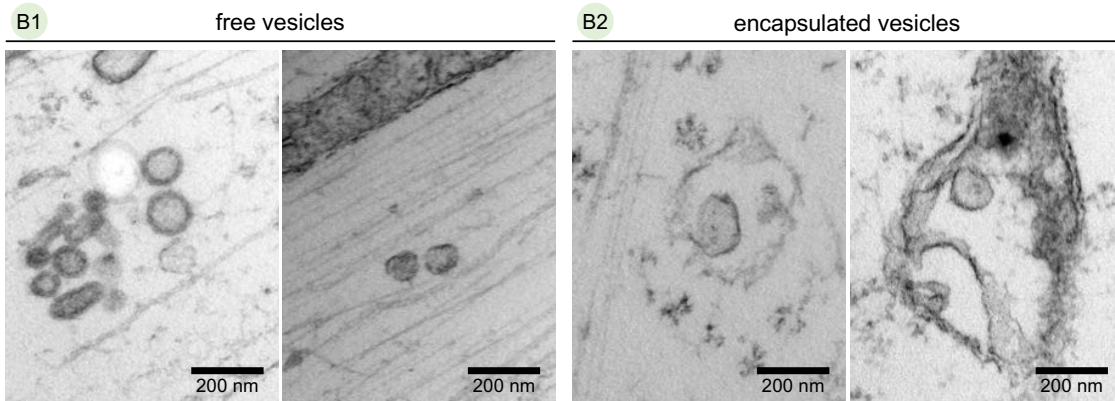


Figure 7: **Internalization of ASC-EVs in SCs.** The interaction mechanism of ASC-EVs with SCs was studied with confocal microscopy and transmission electron microscopy. **A1)** Confocal microscopy showed PKH67-labeled EVs (green) inside the SCs' membrane stained for NGFR (magenta). EVs were observed either single at the cellular processes, or accumulated in the nuclear (grey) vicinity. **A2)** Cross sections of reconstructed z-stacks confirmed internalization of ASC-EVs. **B)** Electron microscopy was used for more detailed analysis of structures involved in the internalization. Potential EVs were identified inside the SC processes without an encapsulating membrane (**B1**) or inside another lumen (**B2**).

### 3.2.1 Internalization of ASC-EVs by SCs is energy-dependent

After determining internalization and subsequent intracellular translocation of EVs, energy-dependence of the membrane transit was tested. Therefore, SCs were deprived of energy by diminishing metabolism at 4°C or inhibition of the mitochondrial respiration with sodium azide. SCs were pretreated for 30 min prior to EV treatment for 30 min. Scanning electron micrographs revealed that at 37°C, EVs were no longer present at the cell surface (figure 8A), suggesting complete internalization within 30 min. When cooled to 4°C, EVs associated with the SCs' membrane were found (figure 8B), however, some EVs seemed to be enveloped by a membrane as seen in figure 8B2. Hence, the internalization of EVs was diminished and slowed at low temperatures. When mitochondrial respiration was impeded and the cell deprived of its energy, any energy-dependent internalization was suppressed as seen in figure 8C. Vesicular structures with inhomogenous size range (<20 nm to 2 µm) were attached to the membrane surface, without visible internalization. The accumulation of vesicles at the membrane and complete block of internalization strongly suggests energy-dependent internalization mechanisms of small EVs.

### 3.2.2 Internalization of ASC-EVs by SCs is mostly mediated by clathrin

After establishing the energy-dependence of EV internalization, biochemical inhibitors were used to narrow down potential routes of internalization. To this end, SCs were pretreated with inhibitors prior to incubation with EVs for 3 hours in the presence of inhibitors. Then, internalization was qualitatively assessed and quantified via imaging flow cytometry, to combine qualitative powers of microscopy with the semiquantitative power of flow cytometry. First, MβCD was used to deplete SCs of cholesterol, and thereby inhibit clathrin-independent endocytosis. As the depletion of cholesterol may interfere with CME and MP, the CCP-formation interceptor CPZ was used to impede CME, and MP was blocked by the sodium/hydrogen exchanger EIPA. When comparing the normalized number of cells associated with PKH-signal of inhibitor-treated SCs to untreated SCs, neither CPZ nor EIPA treatment resulted in a significant change of cells associated with PKH<sup>+</sup> EVs (see figures 9B and 10B). However, further analysis of internalization revealed significant differences in EV uptake. The internalization score, a measure of internalization quality, of CPZ-treated SCs decreased dose-dependently, with significant reduction of internalization at 25 µM to  $0.822 \pm 0.099$  - fold compared to untreated SCs (see figure 9C). When comparing the quantitative internalization measure, the spot count, of CPZ-treated SCs with untreated SCs, a more drastic dose-dependent reduction of internalized EVs emerges. Normalized to untreated SCs, the spot count decreased highly significant to  $0.481 \pm 0.169$  fold when treated with 25 µM CPZ, as depicted in figure 9D. Even at lower concentrations internalization quantity could be significantly reduced, as treatment with 5 µM CPZ resulted in a  $0.703 \pm 0.138$  times decrease of the spot count, and further to  $0.666 \pm 0.042$  when treated with 10 µM CPZ. An involvement of clathrin in the internalization of ASC-derived small EVs can thereby be deduced.

### Energy-Dependence of ASC-EV Internalization in SCs

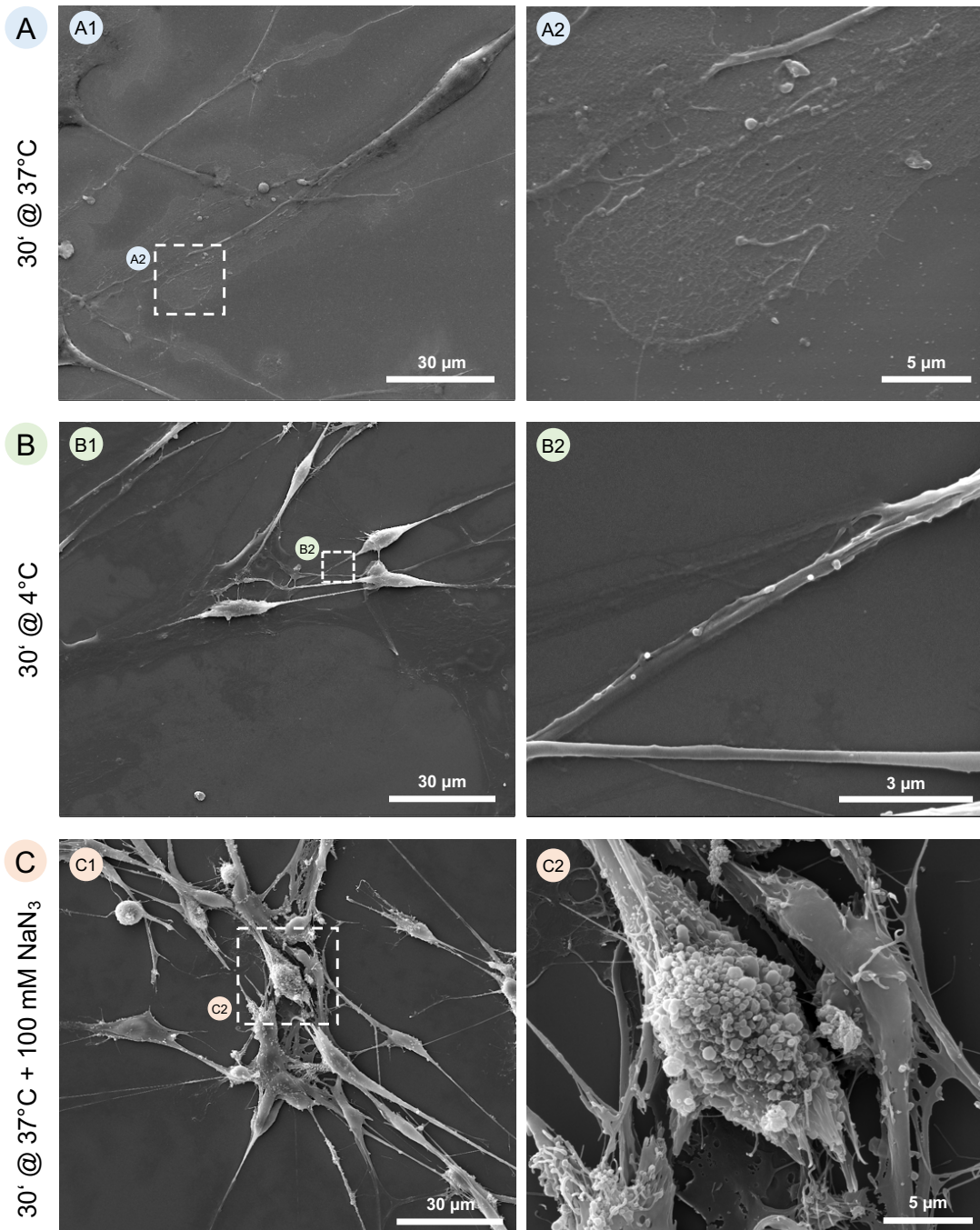


Figure 8: **Energy-dependence of ASC-EV internalization in SCs.** SCs were treated with EVs for 30 min at 37°C (A), 4°C (B) or energy-deprived with sodium azide (C) to investigate the energy-dependence of EV internalization. Right images show regions of interest with higher magnification.

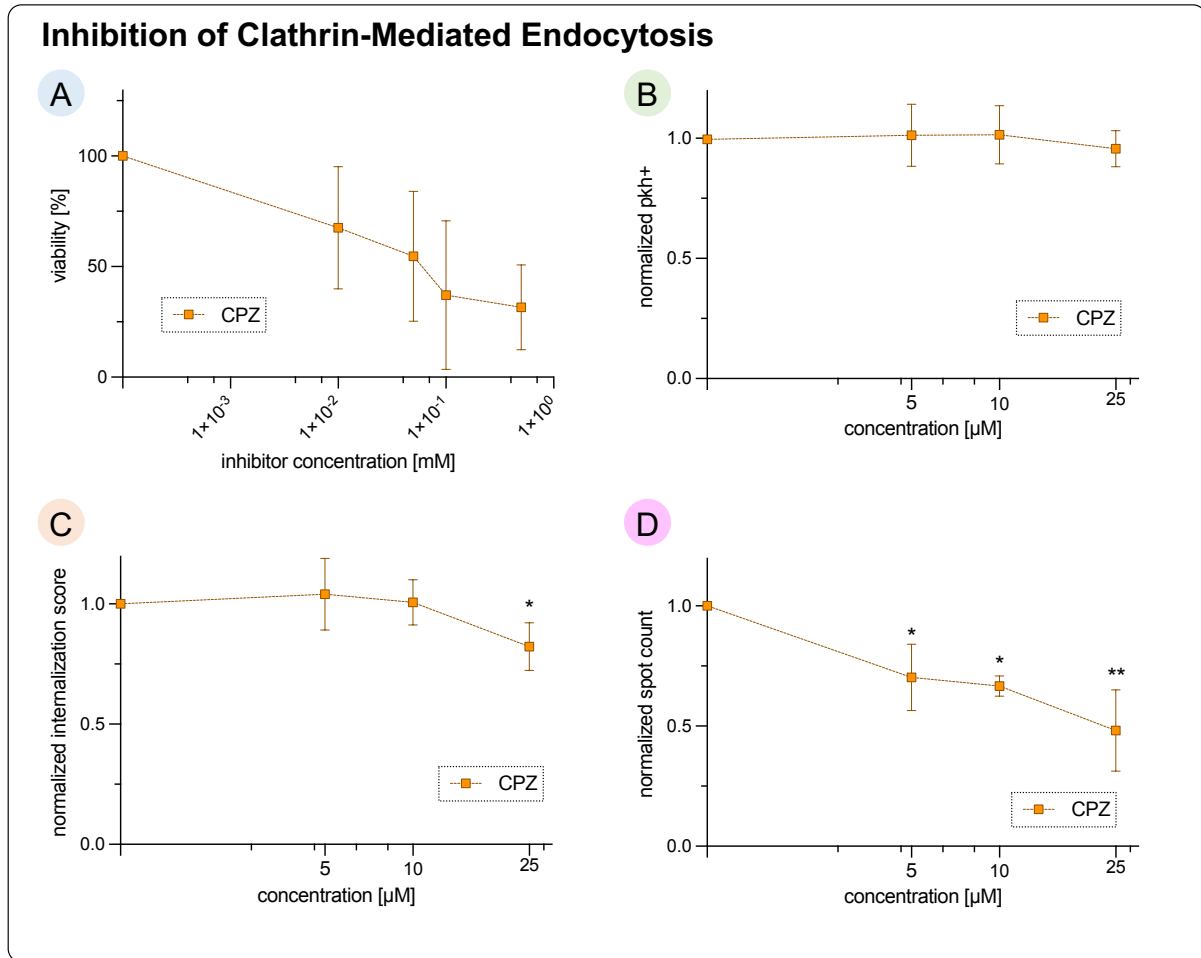


Figure 9: **Inhibition of clathrin-mediated endocytosis.** CME was inhibited with CCP-formation blocker CPZ. **A)** Cytotoxicity of CPZ. **B)** Dose-dependent normalized fraction of SCs associated with PKH67-labeled EVs. **C)** Dose-dependent normalized internalization score of EVs. **D)** Dose-dependent normalized spot count of EVs. Values plotted as mean value  $\pm$  standard deviation. Significance when compared to controls shown by \*\* =  $p < 0.01$ , \* =  $p < 0.05$ .

A further analysis of the internalization quality of EVs by SCs when blocking MP showed a significant reduction of internalization quality. When treated with 50  $\mu$ M EIPA, the internalization score was significantly diminished to  $0.850 \pm 0.084$  times compared to the untreated control (see figure 10C). By treatment with 100  $\mu$ M EIPA, the internalization quality was further reduced to  $0.799 \pm 0.184$  times the control. Investigating the internalization quantity, EIPA treatment up to 100  $\mu$ M did not yield significant changes of EV internalization spot count (see figure 10D).

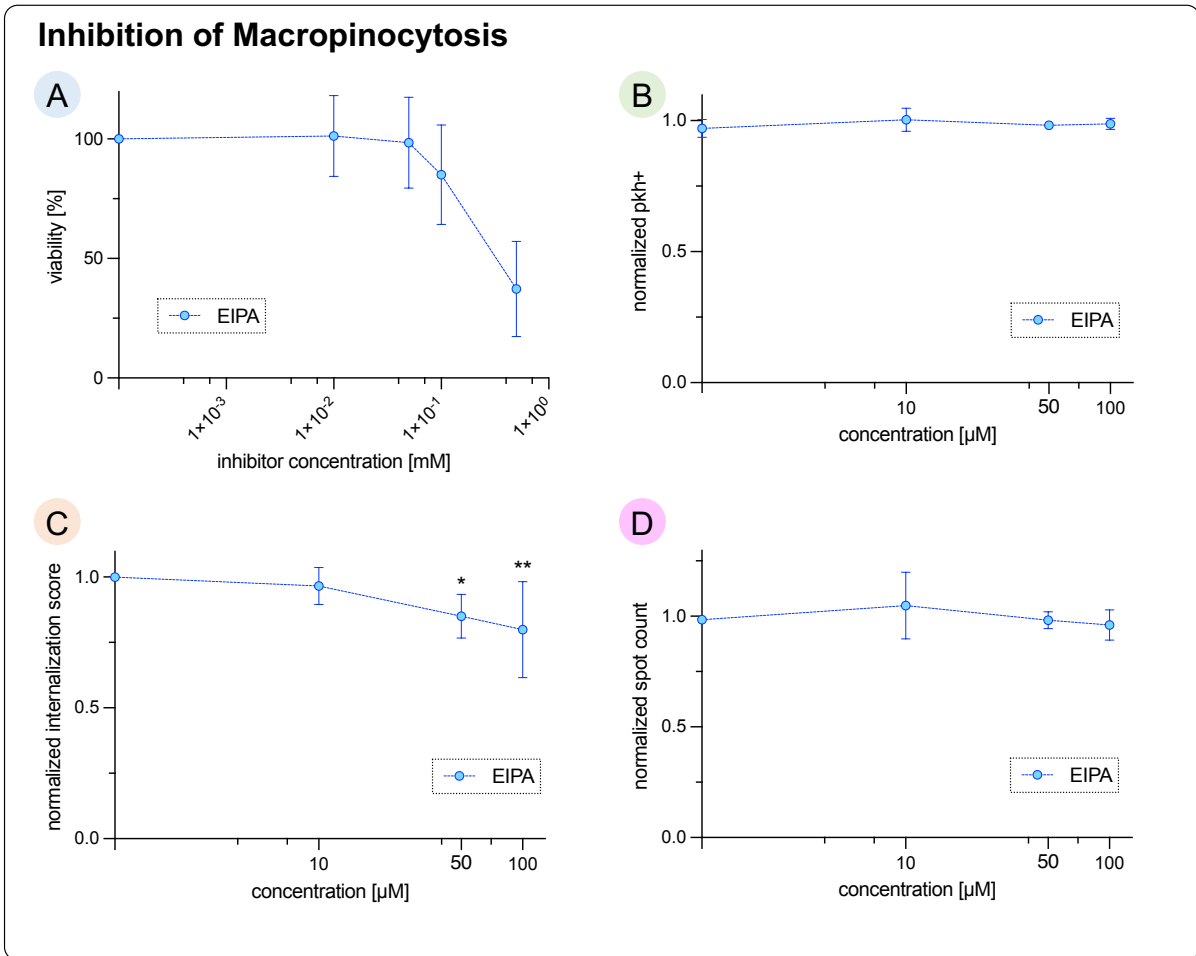


Figure 10: **Inhibition of macropinocytosis.** MP was inhibited with CCP-blocker CPZ. **A)** Cytotoxicity of CPZ. **B)** Dose-dependent normalized fraction of SCs associated with PKH67-labeled EVs. **C)** Dose-dependent normalized internalization score of EVs. **D)** Dose-dependent normalized spot count of EVs. Values plotted as mean value  $\pm$  standard deviation. \*\* =  $p < 0.01$ , \* =  $p < 0.05$

## 4 Discussion

Depending on the severity of the injury, the peripheral nervous system has remarkable intrinsic regeneration capabilities. But certain injuries require surgical intervention, and may require grafting of nervous tissue, or alternative nerve guidance structures. However, commercially available nerve guidance conduits fall short of the success of autologous nerve grafts [83]. Modern alternative therapeutic approaches founded on the understanding of underlying cellular mechanisms aim at supporting the axonal regeneration. And while EVs may not replace surgery of long distance defects, they harbor the potential to activate endogenous neurotrophic processes, and thereby improve non-surgical peripheral nerve regeneration in relatively mild cases of PNI, and aid axonal regeneration following surgical nerve repair tremendously.

However, the intercellular cargo transfer system of EVs is yet to be fully characterized and understood. In 2019, Margolis *et al.* published eight challenges that need to be addressed in order to harness the full therapeutic and diagnostic potential of EVs [17]. This study aimed at adding to the knowledge necessary to solve the sixth challenge, the delivery of EVs to target cells.

The modes of interaction between EVs and target cells are manifold and depend on cell type and condition, however, in the setting of ASC-EVs interacting with repair-phenotype SCs, internalization and nuclear translocation has been shown [16]. While internalization of ASC-EVs by SCs has been previously reported [84, 85], these investigations lack sophisticated methodology and base their assumptions on 2D microscopy. Study designs focusing on EV-mediated effects often fail to further characterize the interaction between EVs and target cells. Hence, this study characterizes the transit of ASC-EVs through SCs' cell membrane. To this end, small EVs were isolated from cell culture supernatant of ASCs via established differential ultracentrifugation. ASC-EVs were then characterized according to the current guidelines [22]. To approximate the size distribution and concentration, nanoparticle tracking analysis was used. Further, immunophenotyping was performed with imaging flow cytometry, allowing analysis on a single vesicle resolution [86].

First, the energy-dependence of the transit and its temperature sensitivity was confirmed, in line with the current literature [51–53, 87]. Upon applying a temperature block, EVs could be visualized adsorbed to the SCs' membrane without internalization. Prior to internalization, EVs interact with membrane proteins on the receptor cell and drift along filopodia on the cellular membrane, a process known from viral membrane transit. This filopodia surfing relocates EVs towards the cell body, and are sites known for actin remodeling activity, and hence hotspots of endocytosis [88, 89].

Further, the internalization of EVs was qualitatively and quantitatively assessed. While confocal microscopy is well suited for the qualitative analysis of EV internalization, it lacks quantitative power for statistical analysis. Flow cytometry on the other hand provides semiquantitative results, however, it lacks the spatial resolution for qualitative analysis. With conventional flow cytometry, it is also difficult to distinguish between vesicles adsorbed to the membrane, or fully internalized vesicles, as calculations are based on fluorescence intensities without respect to spacial localization. To combine the best of both worlds, the internalization of EVs by SCs was investigated with imaging flow cytometry, a method well suited for internalization studies of small particles and vesicles [87, 90]. Fluorescently labeled ASC-EVs were incubated with either pretreated SCs in the presence of inhibitors, or untreated SCs in standard culture medium. Internalization quality and quantity was characterized with two scores, the internalization score and spot count, respectively. By determining the colocalization index of an eroded mask based on the brightfield image of the cell with the PKH67 signal, a qualitative assessment of the EV internalization was possible. To determine the internalization quantity, fluorescence intensity hotspots within the cell were counted and reported as spot count. While inhibition of MP did not alter the internalization of EVs, SCs treated with CME inhibitor CPZ could internalize only half

the amount of EVs, compared to untreated SCs. This led to the assumption that in SCs, the internalization of ASC-EVs is mostly clathrin dependent. An ever-increasing body of evidence suggests that CME may indeed be the pivotal mode EV internalization [52, 53, 90]. Controversially, glial cells of the central nervous system have been shown to internalize EVs mostly via MP [91], further underlining that modes of interaction depend on the cell type. A complete block of ASC-EV internalization could neither be achieved with EIPA nor CPZ alone, suggesting additional modes of membrane transit, which have not been investigated, are involved in the internalization of EVs in SCs. However, whether these alternative cellular entry modes are activated upon inhibition of CCP formation and act as rescue pathways, or contribute independently from each other to the internalization of different subpopulations of EVs remains unknown. In HeLa cervical cancer cells, Verdera *et al.* have identified two modes of EV internalization that act independently from each other [52]. Within SCs' processes, EVs were identified both with and without enclosing membrane, further supporting the hypothesis of more than one modes of internalization. Additionally, the investigation was carried out with a rather heterogenous population of EVs, isolated solely on their density and size. It has been previously suggested that various subtypes of EVs use different routes of internalization, or even a different mode of interaction altogether [51]. While EV heterogeneity is dependent on the cells of origin, the type of recipient cell and its metabolic state cannot be neglected, as it has been reported that the internalization is more dependent on the recipient cell than the cells of origin [92]. To get a better understanding of factors determining modes of interaction, more sophisticated EV isolation and purification methods need to be established. While size and surface proteins may seem obvious factors which determine the interaction, it is unknown what role the EV cargo and immunophenotype play in interaction determination [93]. Prior to internalization, EV recognition occurs through interactions between proteins on both EV and target cell membrane [51]. This initial interaction is pivotal in determining the fate of the EV, as cleavage of EV membrane proteins can drastically reduce the internalization of EVs [70]. Recent therapeutic approaches aim at enhancing EV internalization by engineering EV membrane proteins, such as the hallmark EV surface marker CD81 [94, 95].

The therapeutic potential of ASC-EVs in peripheral nerve regeneration has been shown several times, however, it remains unclear how ASC-EVs exert their proregenerative effects. Based on previous investigations suggesting ASC-EVs are internalized by SCs [16], this study provides first evidence that the internalization of ASC-EVs by SCs is energy-dependent and mediated by clathrin. However, it is likely that EVs may be internalized via more than one route, depending on multiple factors that are yet to be fully characterized. Furthermore, fate of EVs following internalization is mostly undescribed. Internalization does not necessarily mean cargo delivery, as EVs need to evade the endolysosomal degradation, have to be unpacked and require translocation to their yet unknown final destination.

## Outlook

As previously mentioned, inhibition of CME resulted in a significant reduction of EV-internalization, however, it did not fully block membrane transit, suggesting additional modes of internalization that require investigation. By depleting the cell membrane of cholesterol, M $\beta$ CD can be used to investigate cholesterol-dependent, clathrin-independent modes of internalization. Additionally, different internalization mechanisms, both clathrin dependent and independent, require the GTPase dynamin to complete internalization. Inhibition of dynamin with the inhibitor dynasore may provide further insight into the requirements for internalization of ASC-EVs.

The findings of CME involvement in ASC-EV internalization may be validated with Pitstop2, which binds competitively to the clathrin heavy chain (CHC) and thereby prevents CME. Nevertheless, the biochemical inhibition of elementary processes, such as endocytosis, is not without challenges. Off-target effects and unspecific inhibition can distort readouts, alter cellular behaviour and subsequently lead to misinterpretation. It is therefore advisable to further confirm the findings of inhibitor studies with additional assays, such as post-transcriptional gene silencing followed by rescue experiments.

In figure 7B, vesicular structures of roughly 100 nm with lipid bilayer were identified within the SCs. However, transmission electron microscopy lacks the specificity to unambiguously discriminate internalized ASC-EVs from other vesicular structures of similar size. To overcome this hurdle, a combined approach of high resolution fluorescence microscopy and transmission electron microscopy, termed correlated light and electron microscopy (CLEM), is currently being adapted in cooperation with the Electron Microscopy Core Facility of the Vienna Biocenter. Recent advances in technology may allow integration of live cell imaging into the CLEM investigation, extending the information gathered by another dimension.

The interdisciplinary field of EV research is everexpanding. A growing body of knowledge and advances in technology will constantly drive the effort to decipher the intriguing messenger system of extracellular vesicles.

## Bibliography

- [1] E. O. Johnson, A. B. Zoubos, and P. N. Soucacos, "Regeneration and repair of peripheral nerves," *Injury*, vol. 36, no. 4, pp. S24–S29, nov 2005. [Online]. Available: <https://doi.org/10.1016%2Fj.injury.2005.10.012>
- [2] V. Hasirci, D. Arslantunali, T. Dursun, D. Yucel, and N. Hasirci, "Peripheral nerve conduits: technology update," *Medical Devices: Evidence and Research*, vol. 7, pp. 405–424, dec 2014. [Online]. Available: <https://doi.org/10.2147%2Fmder.s59124>
- [3] H. J. SEDDON, "THREE TYPES OF NERVE INJURY," *Brain*, vol. 66, no. 4, pp. 237–288, 12 1943. [Online]. Available: <https://doi.org/10.1093/brain/66.4.237>
- [4] A. Baradaran, H. El-Hawary, J. I. Efanov, and L. Xu, "Peripheral nerve healing: So near and yet so far," *Seminars in Plastic Surgery*, vol. 35, no. 03, pp. 204–210, aug 2021. [Online]. Available: <https://doi.org/10.1055%2Fs-0041-1731630>
- [5] T. Gordon, "Peripheral nerve regeneration and muscle reinnervation," *Int J Mol Sci*, vol. 21, no. 22, p. 8652, nov 2020. [Online]. Available: <https://doi.org/10.3390%2Fijms21228652>
- [6] K. R. Jessen and R. Mirsky, "The success and failure of the schwann cell response to nerve injury," *Frontiers in Cellular Neuroscience*, vol. 13, Feb 2019. [Online]. Available: <http://dx.doi.org/10.3389/fncel.2019.00033>
- [7] —, "The repair schwann cell and its function in regenerating nerves," *The Journal of Physiology*, vol. 594, no. 13, pp. 3521–3531, Mar 2016. [Online]. Available: <http://dx.doi.org/10.1113/JP270874>
- [8] O. A. Sulaiman and T. Gordon, "ROLE OF CHRONIC SCHWANN CELL DENERVATION IN POOR FUNCTIONAL RECOVERY AFTER NERVE INJURIES AND EXPERIMENTAL STRATEGIES TO COMBAT IT," *Neurosurgery*, vol. 65, no. suppl\_4, pp. A105–A114, oct 2009. [Online]. Available: <https://doi.org/10.1227%2F01.neu.0000358537.30354.63>
- [9] G. Nocera and C. Jacob, "Mechanisms of schwann cell plasticity involved in peripheral nerve repair after injury," *Cellular and Molecular Life Sciences*, vol. 77, no. 20, pp. 3977–3989, apr 2020. [Online]. Available: <https://doi.org/10.1007%2Fs00018-020-03516-9>
- [10] S. Bolivar, X. Navarro, and E. Udina, "Schwann cell role in selectivity of nerve regeneration," *Cells*, vol. 9, no. 9, p. 2131, sep 2020. [Online]. Available: <https://doi.org/10.3390%2Fcells9092131>

- [11] F. Millesi, T. Weiss, A. Mann, M. Haertinger, L. Semmler, P. Supper, D. Pils, A. Naghilou, and C. Radtke, "Defining the regenerative effects of native spider silk fibers on primary schwann cells, sensory neurons, and nerve-associated fibroblasts," *The FASEB Journal*, vol. 35, no. 2, nov 2020. [Online]. Available: <https://doi.org/10.1096%2Fj.202001447r>
- [12] A. D. Levi, S. S. Burks, K. D. Anderson, M. Dididze, A. Khan, and W. D. Dietrich, "The use of autologous schwann cells to supplement sciatic nerve repair with a large gap: First in human experience," *Cell Transplantation*, vol. 25, no. 7, pp. 1395–1403, jul 2016. [Online]. Available: <https://doi.org/10.3727%2F096368915x690198>
- [13] A. Faroni, G. Terenghi, and A. J. Reid, "Adipose-derived stem cells and nerve regeneration," in *International Review of Neurobiology*. Elsevier, 2013, pp. 121–136. [Online]. Available: <https://doi.org/10.1016%2Fb978-0-12-410499-0.00005-8>
- [14] F. M. Walocko, R. K. Khouri, M. G. Urbanek, B. Levi, and P. S. Cederna, "The potential roles for adipose tissue in peripheral nerve regeneration," *Microsurgery*, vol. 36, no. 1, pp. 81–88, sep 2015. [Online]. Available: <https://doi.org/10.1002%2Fmicr.22480>
- [15] E. R. Abels and X. O. Breakefield, "Introduction to extracellular vesicles: Biogenesis, rna cargo selection, content, release, and uptake," *Cellular and Molecular Neurobiology*, vol. 36, no. 3, pp. 301–312, Apr 2016. [Online]. Available: <http://dx.doi.org/10.1007/s10571-016-0366-z>
- [16] M. Haertinger, T. Weiss, A. Mann, A. Tabi, V. Brandel, and C. Radtke, "Adipose stem cell-derived extracellular vesicles induce proliferation of schwann cells via internalization," *Cells*, vol. 9, no. 1, p. 163, jan 2020. [Online]. Available: <https://doi.org/10.3390%2Fcells9010163>
- [17] L. Margolis and Y. Sadovsky, "The biology of extracellular vesicles: The known unknowns," *PLOS Biology*, vol. 17, no. 7, p. e3000363, jul 2019. [Online]. Available: <https://doi.org/10.1371%2Fjournal.pbio.3000363>
- [18] P. Wolf, "The nature and significance of platelet products in human plasma," *British Journal of Haematology*, vol. 13, no. 3, pp. 269–288, may 1967. [Online]. Available: <https://doi.org/10.1111%2Fj.1365-2141.1967.tb08741.x>
- [19] G. van Niel, G. D'Angelo, and G. Raposo, "Shedding light on the cell biology of extracellular vesicles," *Nature Reviews Molecular Cell Biology*, vol. 19, no. 4, pp. 213–228, jan 2018. [Online]. Available: <https://doi.org/10.1038%2Fnmr.2017.125>
- [20] S. EL Andaloussi, I. Mäger, X. O. Breakefield, and M. J. A. Wood, "Extracellular vesicles: biology and emerging therapeutic opportunities," *Nat Rev Drug Discov*, vol. 12, no. 5, pp. 347–57, May 2013.

- [21] M. Z. Ratajczak and J. Ratajczak, “Extracellular microvesicles/exosomes: discovery, disbelief, acceptance, and the future?” *Leukemia*, vol. 34, no. 12, pp. 3126–3135, sep 2020. [Online]. Available: <https://doi.org/10.1038%2Fs41375-020-01041-z>
- [22] C. Théry, K. W. Witwer, E. Aikawa, M. J. Alcaraz, J. D. Anderson, R. Andriantsitohaina, A. Antoniou, T. Arab, F. Archer, G. K. Atkin-Smith, and et al., “Minimal information for studies of extracellular vesicles 2018 (misev2018): a position statement of the international society for extracellular vesicles and update of the misev2014 guidelines,” *Journal of Extracellular Vesicles*, vol. 7, no. 1, p. 1535750, Nov 2018. [Online]. Available: <http://dx.doi.org/10.1080/20013078.2018.1535750>
- [23] M. Battistelli and E. Falcieri, “Apoptotic bodies: Particular extracellular vesicles involved in intercellular communication,” *Biology*, vol. 9, no. 1, p. 21, jan 2020. [Online]. Available: <https://doi.org/10.3390%2Fbiology9010021>
- [24] L. Witte and J. C. Gross, “Extracellular vesicles – developmental messengers of tissue crosstalk,” *Trillium Extracellular Vesicles*, vol. 1, no. 1, pp. 31–35, nov 2019. [Online]. Available: <https://doi.org/10.47184%2Ftev.2019.01.04>
- [25] L. Cruz, J. A. A. Romero, R. P. Iglesia, and M. H. Lopes, “Extracellular vesicles: Decoding a new language for cellular communication in early embryonic development,” *Frontiers in Cell and Developmental Biology*, vol. 6, aug 2018. [Online]. Available: <https://doi.org/10.3389%2Ffcell.2018.00094>
- [26] I. J. McGough and J.-P. Vincent, “Exosomes in developmental signalling,” *Development*, vol. 143, no. 14, pp. 2482–2493, jul 2016. [Online]. Available: <https://doi.org/10.1242%2Fdev.126516>
- [27] M. Danilchik and T. Tumarkin, “Exosomal trafficking inXenopusdevelopment,” *genesis*, vol. 55, no. 1-2, p. e23011, jan 2017. [Online]. Available: <https://doi.org/10.1002%2Fdvg.23011>
- [28] E. A. Mellisho, A. E. Velásquez, M. J. Nuñez, J. G. Cabezas, J. A. Cueto, C. Fader, F. O. Castro, and L. Rodríguez-Álvarez, “Identification and characteristics of extracellular vesicles from bovine blastocysts produced in vitro,” *PLOS ONE*, vol. 12, no. 5, p. e0178306, may 2017. [Online]. Available: <https://doi.org/10.1371%2Fjournal.pone.0178306>
- [29] S. L. N. Maas, X. O. Breakefield, and A. M. Weaver, “Extracellular vesicles: Unique inter-cellular delivery vehicles,” *Trends Cell Biol*, vol. 27, no. 3, pp. 172–188, 03 2017.
- [30] P. D. Stahl and G. Raposo, “Extracellular vesicles: Exosomes and microvesicles, integrators of homeostasis,” *Physiology*, vol. 34, no. 3, pp. 169–177, may 2019. [Online]. Available: <https://doi.org/10.1152%2Fphysiol.00045.2018>

- [31] X. Chang, S.-L. Wang, S.-B. Zhao, Y.-H. Shi, P. Pan, L. Gu, J. Yao, Z.-S. Li, and Y. Bai, "Extracellular vesicles with possible roles in gut intestinal tract homeostasis and IBD," *Mediators of Inflammation*, vol. 2020, pp. 1–14, jan 2020. [Online]. Available: <https://doi.org/10.1155%2F2020%2F1945832>
- [32] J. D. Hutcheson and E. Aikawa, "Extracellular vesicles in cardiovascular homeostasis and disease," *Current Opinion in Cardiology*, vol. 33, no. 3, pp. 290–297, may 2018. [Online]. Available: <https://doi.org/10.1097%2Fhco.0000000000000510>
- [33] J. P. Nederveen, G. Warnier, A. D. Carlo, M. I. Nilsson, and M. A. Tarnopolsky, "Extracellular vesicles and exosomes: Insights from exercise science," *Frontiers in Physiology*, vol. 11, feb 2021. [Online]. Available: <https://doi.org/10.3389%2Ffphys.2020.604274>
- [34] D. C. Bittel and J. K. Jaiswal, "Contribution of extracellular vesicles in rebuilding injured muscles," *Frontiers in Physiology*, vol. 10, jul 2019. [Online]. Available: <https://doi.org/10.3389%2Ffphys.2019.00828>
- [35] S. Taverna, M. Pucci, and R. Alessandro, "Extracellular vesicles: small bricks for tissue repair/regeneration," *Annals of Translational Medicine*, vol. 5, no. 4, pp. 83–83, feb 2017. [Online]. Available: <https://doi.org/10.21037%2Fatm.2017.01.53>
- [36] E. Feigerlová, S.-F. Battaglia-Hsu, T. Hauet, and J.-L. Guéant, "Extracellular vesicles as immune mediators in response to kidney injury," *American Journal of Physiology-Renal Physiology*, vol. 314, no. 1, pp. F9–F21, jan 2018. [Online]. Available: <https://doi.org/10.1152%2Fajprenal.00336.2017>
- [37] T. M. Bui, L. A. Mascarenhas, and R. Sumagin, "Extracellular vesicles regulate immune responses and cellular function in intestinal inflammation and repair," *Tissue Barriers*, vol. 6, no. 2, p. e1431038, feb 2018. [Online]. Available: <https://doi.org/10.1080%2F21688370.2018.1431038>
- [38] G. Su, X. Ma, and H. Wei, "Multiple biological roles of extracellular vesicles in lung injury and inflammation microenvironment," *BioMed Research International*, vol. 2020, pp. 1–6, jul 2020. [Online]. Available: <https://doi.org/10.1155%2F2020%2F5608382>
- [39] P. D. Robbins and A. E. Morelli, "Regulation of immune responses by extracellular vesicles," *Nature Reviews Immunology*, vol. 14, no. 3, pp. 195–208, feb 2014. [Online]. Available: <https://doi.org/10.1038%2Fnri3622>
- [40] Z. Chen, A. T. Larregina, and A. E. Morelli, "Impact of extracellular vesicles on innate immunity," *Current Opinion in Organ Transplantation*, vol. 24, no. 6, pp. 670–678, dec 2019. [Online]. Available: <https://doi.org/10.1097%2Fmot.0000000000000701>

- [41] J. Holtzman and H. Lee, "Emerging role of extracellular vesicles in the respiratory system," *Experimental & Molecular Medicine*, vol. 52, no. 6, pp. 887–895, jun 2020. [Online]. Available: <https://doi.org/10.1038%2Fs12276-020-0450-9>
- [42] T. J. Brown and V. James, "The role of extracellular vesicles in the development of a cancer stem cell microenvironment niche and potential therapeutic targets: A systematic review," *Cancers*, vol. 13, no. 10, p. 2435, may 2021. [Online]. Available: <https://doi.org/10.3390%2Fcancers13102435>
- [43] Z. Qian, Q. Shen, X. Yang, Y. Qiu, and W. Zhang, "The role of extracellular vesicles: An epigenetic view of the cancer microenvironment," *BioMed Research International*, vol. 2015, pp. 1–8, 2015. [Online]. Available: <https://doi.org/10.1155%2F2015%2F649161>
- [44] H. Peinado, M. Alečković, S. Lavotshkin, I. Matei, B. Costa-Silva, G. Moreno-Bueno, M. Hergueta-Redondo, C. Williams, G. García-Santos, C. M. Ghajar, A. Nitadori-Hoshino, C. Hoffman, K. Badal, B. A. Garcia, M. K. Callahan, J. Yuan, V. R. Martins, J. Skog, R. N. Kaplan, M. S. Brady, J. D. Wolchok, P. B. Chapman, Y. Kang, J. Bromberg, and D. Lyden, "Melanoma exosomes educate bone marrow progenitor cells toward a pro-metastatic phenotype through MET," *Nature Medicine*, vol. 18, no. 6, pp. 883–891, may 2012. [Online]. Available: <https://doi.org/10.1038%2Fnm.2753>
- [45] N. Tominaga, N. Kosaka, M. Ono, T. Katsuda, Y. Yoshioka, K. Tamura, J. Lötvall, H. Nakagama, and T. Ochiya, "Brain metastatic cancer cells release microRNA-181c-containing extracellular vesicles capable of destructing blood–brain barrier," *Nature Communications*, vol. 6, no. 1, apr 2015. [Online]. Available: <https://doi.org/10.1038%2Fncomms7716>
- [46] W. Hu, C. Liu, Z.-Y. Bi, Q. Zhou, H. Zhang, L.-L. Li, J. Zhang, W. Zhu, Y.-Y.-Y. Song, F. Zhang, H.-M. Yang, Y.-Y. Bi, Q.-Q. He, G.-J. Tan, C.-C. Sun, and D.-J. Li, "Comprehensive landscape of extracellular vesicle-derived RNAs in cancer initiation, progression, metastasis and cancer immunology," *Molecular Cancer*, vol. 19, no. 1, jun 2020. [Online]. Available: <https://doi.org/10.1186%2Fs12943-020-01199-1>
- [47] F. Teng and M. Fussenegger, "Shedding light on extracellular vesicle biogenesis and bioengineering," *Advanced Science*, vol. 8, no. 1, p. 2003505, nov 2020. [Online]. Available: <https://doi.org/10.1002%2Fadvs.202003505>
- [48] F. Zeng and A. E. Morelli, "Extracellular vesicle-mediated MHC cross-dressing in immune homeostasis, transplantation, infectious diseases, and cancer," *Seminars in Immunopathology*, vol. 40, no. 5, pp. 477–490, mar 2018. [Online]. Available: <https://doi.org/10.1007%2Fs00281-018-0679-8>
- [49] M. F. Lindenbergh and W. Stoorvogel, "Antigen presentation by extracellular vesicles from professional antigen-presenting cells," *Annual Review of Immunology*,

- vol. 36, no. 1, pp. 435–459, apr 2018. [Online]. Available: <https://doi.org/10.1146%2Fannurev-immunol-041015-055700>
- [50] I. Prada and J. Meldolesi, “Binding and fusion of extracellular vesicles to the plasma membrane of their cell targets,” *International Journal of Molecular Sciences*, vol. 17, no. 8, p. 1296, aug 2016. [Online]. Available: <https://doi.org/10.3390%2Fijms17081296>
- [51] L. A. Mulcahy, R. C. Pink, and D. R. F. Carter, “Routes and mechanisms of extracellular vesicle uptake,” *Journal of Extracellular Vesicles*, vol. 3, no. 1, p. 24641, Jan 2014. [Online]. Available: <http://dx.doi.org/10.3402/jev.v3.24641>
- [52] H. Costa Verdera, J. J. Gitz-Francois, R. M. Schiffelers, and P. Vader, “Cellular uptake of extracellular vesicles is mediated by clathrin-independent endocytosis and macropinocytosis,” *Journal of Controlled Release*, vol. 266, pp. 100–108, 2017. [Online]. Available: <https://www.sciencedirect.com/science/article/pii/S0168365917308520>
- [53] S. Gurung, D. Perocheau, L. Touramanidou, and J. Baruteau, “The exosome journey: from biogenesis to uptake and intracellular signalling,” *Cell Communication and Signaling*, vol. 19, no. 1, apr 2021. [Online]. Available: <https://doi.org/10.1186%2FS12964-021-00730-1>
- [54] K. Laulagnier, C. Javalet, F. J. Hemming, M. Chivet, G. Lachenal, B. Blot, C. Chatellard, and R. Sadoul, “Amyloid precursor protein products concentrate in a subset of exosomes specifically endocytosed by neurons,” *Cellular and Molecular Life Sciences*, vol. 75, no. 4, pp. 757–773, sep 2017. [Online]. Available: <https://doi.org/10.1007%2FS00018-017-2664-0>
- [55] S. Bernardi and C. Balbi, “Extracellular vesicles: From biomarkers to therapeutic tools,” *Biology*, vol. 9, no. 9, p. 258, aug 2020. [Online]. Available: <https://doi.org/10.3390%2Fbiology9090258>
- [56] K. L. Schey, J. M. Luther, and K. L. Rose, “Proteomics characterization of exosome cargo,” *Methods*, vol. 87, pp. 75–82, 2015, the Isolation and Molecular Characterization of Exosomes. [Online]. Available: <https://www.sciencedirect.com/science/article/pii/S1046202315001243>
- [57] S. Ghafouri-Fard, V. Niazi, B. M. Hussen, M. D. Omrani, M. Taheri, and A. Basiri, “The emerging role of exosomes in the treatment of human disorders with a special focus on mesenchymal stem cells-derived exosomes,” *Frontiers in Cell and Developmental Biology*, vol. 9, jul 2021. [Online]. Available: <https://doi.org/10.3389%2Ffcell.2021.653296>
- [58] G. Racchetti and J. Meldolesi, “Extracellular vesicles of mesenchymal stem cells: Therapeutic properties discovered with extraordinary success,” *Biomedicines*, vol. 9, no. 6, p. 667, jun 2021. [Online]. Available: <https://doi.org/10.3390%2Fbiomedicines9060667>

- [59] A. Trzyna and A. Banaś-Ząbczyk, “Adipose-derived stem cells secretome and its potential application in “stem cell-free therapy”,” *Biomolecules*, vol. 11, no. 6, p. 878, jun 2021. [Online]. Available: <https://doi.org/10.3390%2Fbiom11060878>
- [60] H. Alqurashi, I. O. Asencio, and D. W. Lambert, “The emerging potential of extracellular vesicles in cell-free tissue engineering and regenerative medicine,” *Tissue Engineering Part B: Reviews*, dec 2020. [Online]. Available: <https://doi.org/10.1089%2Ften.teb.2020.0222>
- [61] I. M. Bjørge, S. Y. Kim, J. F. Mano, B. Kalionis, and W. Chrzanowski, “Extracellular vesicles, exosomes and shedding vesicles in regenerative medicine - a new paradigm for tissue repair,” *Biomater Sci*, vol. 6, no. 1, pp. 60–78, Dec 2017.
- [62] R. Dong, Y. Liu, Y. Yang, H. Wang, Y. Xu, and Z. Zhang, “MSC-derived exosomes-based therapy for peripheral nerve injury: A novel therapeutic strategy,” *BioMed Research International*, vol. 2019, pp. 1–12, aug 2019. [Online]. Available: <https://doi.org/10.1155%2F2019%2F6458237>
- [63] L. Qing, H. Chen, J. Tang, and X. Jia, “Exosomes and their microrna cargo: New players in peripheral nerve regeneration,” *Neurorehabilitation and Neural Repair*, vol. 32, no. 9, pp. 765–776, Sep 2018. [Online]. Available: <http://dx.doi.org/10.1177/1545968318798955>
- [64] M. Yu, G. Gu, M. Cong, M. Du, W. Wang, M. Shen, Q. Zhang, H. Shi, X. Gu, and F. Ding, “Repair of peripheral nerve defects by nerve grafts incorporated with extracellular vesicles from skin-derived precursor schwann cells,” *Acta Biomaterialia*, jul 2021. [Online]. Available: <https://doi.org/10.1016%2Fj.actbio.2021.07.026>
- [65] M. Lopez-Verrilli, A. Caviedes, A. Cabrera, S. Sandoval, U. Wyneken, and M. Khoury, “Mesenchymal stem cell-derived exosomes from different sources selectively promote neuritic outgrowth,” *Neuroscience*, vol. 320, pp. 129–139, apr 2016. [Online]. Available: <https://doi.org/10.1016%2Fj.neuroscience.2016.01.061>
- [66] Y. Zhang, M. Chopp, X. S. Liu, M. Katakowski, X. Wang, X. Tian, D. Wu, and Z. G. Zhang, “Exosomes derived from mesenchymal stromal cells promote axonal growth of cortical neurons,” *Molecular Neurobiology*, vol. 54, no. 4, pp. 2659–2673, mar 2016. [Online]. Available: <https://doi.org/10.1007%2Fs12035-016-9851-0>
- [67] G. J. Doherty and H. T. McMahon, “Mechanisms of endocytosis,” *Annual Review of Biochemistry*, vol. 78, no. 1, pp. 857–902, jun 2009. [Online]. Available: <https://doi.org/10.1146%2Fannurev.biochem.78.081307.110540>
- [68] M. Kaksonen and A. Roux, “Mechanisms of clathrin-mediated endocytosis,” *Nature Reviews Molecular Cell Biology*, vol. 19, no. 5, pp. 313–326, feb 2018. [Online]. Available: <https://doi.org/10.1038%2Fnmr.2017.132>

- [69] V. Haucke and M. M. Kozlov, "Membrane remodeling in clathrin-mediated endocytosis," *Journal of Cell Science*, vol. 131, no. 17, sep 2018. [Online]. Available: <https://doi.org/10.1242%2Fjcs.216812>
- [70] C. Escrevente, S. Keller, P. Altevogt, and J. Costa, "Interaction and uptake of exosomes by ovarian cancer cells," *BMC Cancer*, vol. 11, no. 1, mar 2011. [Online]. Available: <https://doi.org/10.1186%2F1471-2407-11-108>
- [71] T. Tian, Y.-L. Zhu, Y.-Y. Zhou, G.-F. Liang, Y.-Y. Wang, F.-H. Hu, and Z.-D. Xiao, "Exosome uptake through clathrin-mediated endocytosis and macropinocytosis and mediating miR-21 delivery," *Journal of Biological Chemistry*, vol. 289, no. 32, pp. 22 258–22 267, aug 2014. [Online]. Available: <https://doi.org/10.1074%2Fjbc.m114.588046>
- [72] B. S. Joshi, M. A. de Beer, B. N. G. Giepmans, and I. S. Zuhorn, "Endocytosis of extracellular vesicles and release of their cargo from endosomes," *ACS Nano*, vol. 14, no. 4, pp. 4444–4455, apr 2020. [Online]. Available: <https://doi.org/10.1021%2Facs.nano.9b10033>
- [73] C. Barrès, L. Blanc, P. Bette-Bobillo, S. André, R. Mamoun, H.-J. Gabius, and M. Vidal, "Galectin-5 is bound onto the surface of rat reticulocyte exosomes and modulates vesicle uptake by macrophages," *Blood*, vol. 115, no. 3, pp. 696–705, jan 2010. [Online]. Available: <https://doi.org/10.1182%2Fblood-2009-07-231449>
- [74] K. Sandvig, S. Kavaliauskiene, and T. Skotland, "Clathrin-independent endocytosis: an increasing degree of complexity," *Histochemistry and Cell Biology*, vol. 150, no. 2, pp. 107–118, may 2018. [Online]. Available: <https://doi.org/10.1007%2Fs00418-018-1678-5>
- [75] S. K. Rodal, G. Skretting, Ø. Garred, F. Vilhardt, B. van Deurs, and K. Sandvig, "Extraction of cholesterol with methyl- $\beta$ -cyclodextrin perturbs formation of clathrin-coated endocytic vesicles," *Molecular Biology of the Cell*, vol. 10, no. 4, pp. 961–974, apr 1999. [Online]. Available: <https://doi.org/10.1091%2Fmbc.10.4.961>
- [76] S. Mayor and R. E. Pagano, "Pathways of clathrin-independent endocytosis," *Nature Reviews Molecular Cell Biology*, vol. 8, no. 8, pp. 603–612, aug 2007. [Online]. Available: <https://doi.org/10.1038%2Fnmr2216>
- [77] S. Kumari, S. MG, and S. Mayor, "Endocytosis unplugged: multiple ways to enter the cell," *Cell Research*, vol. 20, no. 3, pp. 256–275, feb 2010. [Online]. Available: <https://doi.org/10.1038%2Fcr.2010.19>
- [78] H.-F. Renard and E. Boucrot, "Unconventional endocytic mechanisms," *Current Opinion in Cell Biology*, vol. 71, pp. 120–129, 2021. [Online]. Available: <https://www.sciencedirect.com/science/article/pii/S0955067421000351>

- [79] J. P. Lim and P. A. Gleeson, "Macropinocytosis: an endocytic pathway for internalising large gulps," *Immunology & Cell Biology*, vol. 89, no. 8, pp. 836–843, mar 2011. [Online]. Available: <https://doi.org/10.1038%2Ficb.2011.20>
- [80] S. Dharmawardhane, A. Schürmann, M. A. Sells, J. Chernoff, S. L. Schmid, and G. M. Bokoch, "Regulation of macropinocytosis by p21-activated kinase-1," *Molecular Biology of the Cell*, vol. 11, no. 10, pp. 3341–3352, oct 2000. [Online]. Available: <https://doi.org/10.1091%2Fmbc.11.10.3341>
- [81] J. L. Stow, Y. Hung, and A. A. Wall, "Macropinocytosis: Insights from immunology and cancer," *Current Opinion in Cell Biology*, vol. 65, pp. 131–140, aug 2020. [Online]. Available: <https://doi.org/10.1016%2Fj.ceb.2020.06.005>
- [82] T. Weiss, S. Taschner-Mandl, P. F. Ambros, and I. M. Ambros, "Detailed protocols for the isolation, culture, enrichment and immunostaining of primary human schwann cells," *Schwann Cells*, pp. 67–86, 2018. [Online]. Available: [http://dx.doi.org/10.1007/978-1-4939-7649-2\\_5](http://dx.doi.org/10.1007/978-1-4939-7649-2_5)
- [83] B. J. Parker, D. I. Rhodes, C. M. O'Brien, A. E. Rodda, and N. R. Cameron, "Nerve guidance conduit development for primary treatment of peripheral nerve transection injuries: A commercial perspective," *Acta Biomaterialia*, vol. 135, pp. 64–86, nov 2021. [Online]. Available: <https://doi.org/10.1016%2Fj.actbio.2021.08.052>
- [84] V. Bucan, D. Vaslaitis, C.-T. Peck, S. Strauß, P. M. Vogt, and C. Radtke, "Effect of exosomes from rat adipose-derived mesenchymal stem cells on neurite outgrowth and sciatic nerve regeneration after crush injury," *Molecular Neurobiology*, vol. 56, no. 3, pp. 1812–1824, jun 2018. [Online]. Available: <https://doi.org/10.1007%2Ffs12035-018-1172-z>
- [85] J. Chen, S. Ren, D. Duscher, Y. Kang, Y. Liu, C. Wang, M. Yuan, G. Guo, H. Xiong, P. Zhan, Y. Wang, H.-G. Machens, and Z. Chen, "Exosomes from human adipose-derived stem cells promote sciatic nerve regeneration via optimizing schwann cell function," *Journal of Cellular Physiology*, vol. 234, no. 12, pp. 23 097–23 110, may 2019. [Online]. Available: <https://doi.org/10.1002%2Fjcp.28873>
- [86] A. Görgens, M. Bremer, R. Ferrer-Tur, F. Murke, T. Tertel, P. A. Horn, S. Thalmann, J. A. Welsh, C. Probst, C. Guerin, C. M. Boulanger, J. C. Jones, H. Hanenberg, U. Erdbrügger, J. Lannigan, F. L. Ricklefs, S. El-Andaloussi, and B. Giebel, "Optimisation of imaging flow cytometry for the analysis of single extracellular vesicles by using fluorescence-tagged vesicles as biological reference material," *Journal of Extracellular Vesicles*, vol. 8, no. 1, p. 1587567, mar 2019. [Online]. Available: <https://doi.org/10.1080%2F20013078.2019.1587567>
- [87] S. Vranic, N. Boggetto, V. Contremoulins, S. Mornet, N. Reinhardt, F. Marano, A. Baeza-Squiban, and S. Boland, "Deciphering the mechanisms of cellular uptake of

- engineered nanoparticles by accurate evaluation of internalization using imaging flow cytometry,” *Particle and Fibre Toxicology*, vol. 10, no. 1, p. 2, 2013. [Online]. Available: <https://doi.org/10.1186%2F1743-8977-10-2>
- [88] T. Tian, Y.-L. Zhu, F.-H. Hu, Y.-Y. Wang, N.-P. Huang, and Z.-D. Xiao, “Dynamics of exosome internalization and trafficking,” *Journal of Cellular Physiology*, vol. 228, no. 7, pp. 1487–1495, mar 2013. [Online]. Available: <https://doi.org/10.1002%2Fjcp.24304>
- [89] W. Heusermann, J. Hean, D. Trojer, E. Steib, S. von Bueren, A. Graff-Meyer, C. Genoud, K. Martin, N. Pizzato, J. Voshol, D. V. Morrissey, S. E. Andaloussi, M. J. Wood, and N. C. Meisner-Kober, “Exosomes surf on filopodia to enter cells at endocytic hot spots, traffic within endosomes, and are targeted to the ER,” *Journal of Cell Biology*, vol. 213, no. 2, pp. 173–184, apr 2016. [Online]. Available: <https://doi.org/10.1083%2Fjcb.201506084>
- [90] C. A. Franzen, P. E. Simms, A. F. V. Huis, K. E. Foreman, P. C. Kuo, and G. N. Gupta, “Characterization of uptake and internalization of exosomes by bladder cancer cells,” *BioMed Research International*, vol. 2014, pp. 1–11, 2014. [Online]. Available: <https://doi.org/10.1155%2F2014%2F619829>
- [91] D. Fitzner, M. Schnaars, D. van Rossum, G. Krishnamoorthy, P. Dibaj, M. Bakhti, T. Regen, U.-K. Hanisch, and M. Simons, “Selective transfer of exosomes from oligodendrocytes to microglia by macropinocytosis,” *Journal of Cell Science*, vol. 124, no. 3, pp. 447–458, feb 2011. [Online]. Available: <https://doi.org/10.1242%2Fjcs.074088>
- [92] S. Horibe, T. Tanahashi, S. Kawauchi, Y. Murakami, and Y. Rikitake, “Mechanism of recipient cell-dependent differences in exosome uptake,” *BMC Cancer*, vol. 18, no. 1, jan 2018. [Online]. Available: <https://doi.org/10.1186%2Fs12885-017-3958-1>
- [93] M. Mathieu, L. Martin-Jaular, G. Lavieu, and C. Théry, “Specificities of secretion and uptake of exosomes and other extracellular vesicles for cell-to-cell communication,” *Nature Cell Biology*, vol. 21, no. 1, pp. 9–17, jan 2019. [Online]. Available: <https://doi.org/10.1038%2Fs41556-018-0250-9>
- [94] D. E. Murphy, O. G. de Jong, M. Brouwer, M. J. Wood, G. Lavieu, R. M. Schiffelers, and P. Vader, “Extracellular vesicle-based therapeutics: natural versus engineered targeting and trafficking,” *Experimental & Molecular Medicine*, vol. 51, no. 3, mar 2019. [Online]. Available: <https://doi.org/10.1038%2Fs12276-019-0223-5>
- [95] S. Vogt, M. R. Bobbili, G. Stadlmayr, K. Stadlbauer, J. Kjems, F. Rüker, J. Grillari, and G. Wozniak-Knopp, “An engineered CD81-based combinatorial library for selecting recombinant binders to cell surface proteins: Laminin binding CD81 enhances cellular uptake of extracellular vesicles,” *Journal of Extracellular Vesicles*, vol. 10, no. 11, sep 2021. [Online]. Available: <https://doi.org/10.1002%2Fjev2.12139>

# List of Figures

Figure 1 **EV biogenesis and interaction.** EVs encapsule bioactive cargo, such as nucleic acids, growth factor proteins, receptors, various antigens or even MHC molecules, and arise from inward budding of the multivesicular body (MVB) membrane. Upon fusion of the MVB-membrane with the cell membrane, EVs are released into the extracellular space, where they act as paracrine or even autocrine messengers. At the target cells, EVs can interact in one or more of several possible ways: 1) immunomodulatory, 2) via receptor binding and subsequent intracellular signaling cascade activation, or 3) by fusion with the plasma membrane, releasing their cargo into the cytoplasm. Additionally, EVs may be 4) internalized via different endocytotic pathways. © Maximilian Haertinger . . . . . 4

Figure 2 **Imaging flow cytometric analysis.** **A)** Gating strategy to determine EV internalization. First, cells in focus (**A1**) were identified and further gated to find single cells (**A2**) and cells with PKH67 signal (**A3**). **B)** EV-internalization quantification by internalization score (**B1**) and spot count inside the cell (**B2**). Multiple subpopulations were identified: SCs with low internalization score and low spot count (**B3**), high internalization score but low spot count (**B4**), low internalization score with high spot count (**B5**), and both high internalization score and high spot count (**B6**). . . . . 16

Figure 3 **Characterization of SCs.** **A)** Immunofluorescence staining of SCs with merged channels (**A1**) and single channels of NGFR (**A2**), THY1 (**A3**) and DAPI (**A4**). **B)** Immunofluorescence staining of SCs with merged channels (**B1**) and single channels of S100 (**B2**), Vimentin (**B3**), DAPI (**B4**) and Sox10 (**B5**). . . . . 17

Figure 4 **Characterization of ASCs.** **A)** Using flow cytometry, marker expression was analyzed. Representative scatter plot (**A1**) and overlay of 8 individual ASC cultures analyzed for their expression of CD29 (**A2**), CD63 (**A3**) and CD90 (**A4**). **B)** Multilineage differentiation potential of primary ASCs. Undifferentiated ASCs in passage 2 (**B1**), adipogenically differentiated ASCs stained with oil red o (**B2**), osteogenically differentiated ASCs stained with alizarin red (**B3**) and chondrogenically differentiated ASCs stained with alcian blue (**B4**). . . . . 18

Figure 5	<b>Characterization of ASC-EVs.</b> <b>A)</b> Schematic depiction of EV isolation process. <b>B)</b> Size distribution histogram of EVs as established with nanoparticle tracking analysis. <b>C)</b> Immunophenotyping of ASC-EVs. Expression analysis scatter plot of tetraspanins CD63 vs. CD81. <b>D)</b> Exemplary imagestream gallery of triple positive ASC-EV: CMG, CD81 and CD63. . . . .	19
Figure 6	<b>Immunophenotyping of ASC-EVs: Gating Strategy.</b> <b>A)</b> Gating strategy to discriminate between calibration beads and vesicles. <b>B)</b> Exemplary image of calibration bead. <b>C)</b> Exemplary image of ASC-EV positive for CMG, CD81 and CD63. . . . .	20
Figure 7	<b>Internalization of ASC-EVs in SCs.</b> The interaction mechanism of ASC-EVs with SCs was studied with confocal microscopy and transmission electron microscopy. <b>A1)</b> Confocal microscopy showed PKH67-labeled EVs (green) inside the SCs' membrane stained for NGFR (magenta). EVs were observed either single at the cellular processes, or accumulated in the nuclear (grey) vicinity. <b>A2)</b> Cross sections of reconstructed z-stacks confirmed internalization of ASC-EVs. <b>B)</b> Electron microscopy was used for more detailed analysis of structures involved in the internalization. Potential EVs were identified inside the SC processes without an encapsulating membrane ( <b>B1</b> ) or inside another lumen ( <b>B2</b> ). . . . .	21
Figure 8	<b>Energy-dependence of ASC-EV internalization in SCs.</b> SCs were treated with EVs for 30 min at 37 °C ( <b>A</b> ), 4 °C ( <b>B</b> ) or energy-deprived with sodium azide ( <b>C</b> ) to investigate the energy-dependence of EV internalization. Right images show regions of interest with higher magnification. . . . .	23
Figure 9	<b>Inhibition of clathrin-mediated endocytosis.</b> CME was inhibited with CCP-formation blocker CPZ. <b>A)</b> Cytotoxicity of CPZ. <b>B)</b> Dose-dependent normalized fraction of SCs associated with PKH67-labeled EVs. <b>C)</b> Dose-dependent normalized internalization score of EVs. <b>D)</b> Dose-dependent normalized spot count of EVs. Values plotted as mean value $\pm$ standard deviation. Significance when compared to controls shown by $** = p < 0.01$ , $* = p < 0.05$ . . . . .	24
Figure 10	<b>Inhibition of macropinocytosis.</b> MP was inhibited with CCP-blocker CPZ. <b>A)</b> Cytotoxicity of CPZ. <b>B)</b> Dose-dependent normalized fraction of SCs associated with PKH67-labeled EVs. <b>C)</b> Dose-dependent normalized internalization score of EVs. <b>D)</b> Dose-dependent normalized spot count of EVs. Values plotted as mean value $\pm$ standard deviation. $** = p < 0.01$ , $* = p < 0.05$ . . . . .	25

# Abbreviations

<b>AF</b>	Alexa Fluor
<b>ASC</b>	Adipose stem cells
<b>AP</b>	Adaptor protein
<b>BAR</b>	Bin/Amphiphysin/Rvs
<b>BDMA</b>	Benzyldimethylamine
<b>BSA</b>	Bovine serum albumin
<b>CCP</b>	Clathrin coated pit
<b>CCV</b>	Clathrin coated vesicle
<b>CD</b>	Cluster of differentiation
<b>CHC</b>	Clathrin heavy chain
<b>CIE</b>	Clathrin independent endocytosis
<b>CLEM</b>	Correlated light and electron microscopy
<b>CLIC/GEEC</b>	Clathrin-independent carrier/glycosylphosphatidylinositol (GPI)-anchored protein enriched endosomal compartments
<b>CMG</b>	Cell Mask Green
<b>CME</b>	Clathrin mediated endocytosis
<b>CPZ</b>	Chlorpromazine
<b>DAPI</b>	4,6-diamidino-2-phenylindole
<b>DDSA</b>	Dodecenylsuccinic anhydride
<b>DMEM</b>	Dulbeccos modified Eagle medium
<b>EDTA</b>	Ethylenediaminetetraacetic acid
<b>EGF</b>	Epidermal growth factor
<b>EIPA</b>	5-(N-Ethyl-N-isopropyl)amilorid

<b>EPS</b>	Epidermal growth factor receptor pathway substrate
<b>EV</b>	Extracellular vesicle
<b>FCS</b>	Fetal calf serum
<b>FEME</b>	Fast endophilin A2-dependent endocytosis
<b>FSC</b>	Forward scatter
<b>GPI-AP</b>	Glycosyl phosphatidylinositol-anchored proteins
<b>GTP</b>	Guanosintriphosphat
<b>HBSS</b>	Hanks balanced salt solution
<b>HEPES</b>	4-(2-hydroxyethyl)-1-piperazineethanesulfonic acid
<b>HMDS</b>	Hexamethyldisilazane
<b>HSC</b>	Heat shock cognate
<b>HSP</b>	Heat shock protein
<b>IFN</b>	Interferon
<b>IL</b>	Interleukin
<b>ISEV</b>	International society for extracellular vesicles
<b>MEM</b>	Modified Eagles medium
<b>MHC</b>	Major histocompatibility complex
<b>MNA</b>	Methylnadic anhydride
<b>MP</b>	Macropinocytosis
<b>MSC</b>	Mesenchymal stem cell
<b>MTT</b>	3-(4,5-Dimethylthiazol-2-yl)-2,5-diphenyltetrazoliumbromid
<b>MVB</b>	Multivesicular body
<b>MVE</b>	Multivesicular endosome
<b>PAK</b>	p21-activated kinase
<b>PBS</b>	Phosphate buffered saline
<b>PDGF</b>	Platelet derived growth factor

<b>PLL</b>	Poly-L-lysine
<b>PNI</b>	Peripheral nerve injury
<b>P/S</b>	Penicillin-streptomycin
<b>RME</b>	Receptor mediated endocytosis
<b>RNA</b>	Ribonucleic acid
<b>RT</b>	Room temperature
<b>SC</b>	Schwann cell
<b>SCEM</b>	Schwann cell expansion medium
<b>SNX</b>	Sorting nexin
<b>SSC</b>	Side scatter
<b>STAT</b>	Signal transducer and activator of transcription
<b>VBC</b>	Vienna biocenter
<b>VBCF</b>	Vienna biocenter core facility